NASA TECHNICAL NOTE

NASA TN D-2032

NASA TN D-2032

A MAGNETICALLY ROTATED ELECTRIC ARC AIR HEATER EMPLOYING A STRONG MAGNETIC FIELD AND COPPER ELECTRODES

by Robert F. Mayo, William L. Wells, and Milton A. Wallio

Langley Research Center
Langley Station, Hampton, Va.

NATIONAL AERONAUTICS AND SPACE ADMINISTRATION • WASHINGTON, D. C. • NOVEMBER 1963

TECHNICAL NOTE D-2032

A MAGNETICALLY ROTATED ELECTRIC ARC AIR HEATER EMPLOYING A STRONG MAGNETIC FIELD AND COPPER ELECTRODES

By Robert F. Mayo, William L. Wells,
and Milton A. Wallio

Langley Research Center
Langley Station, Hampton, Va.

NATIONAL AERONAUTICS AND SPACE ADMINISTRATION

A MAGNETICALLY ROTATED ELECTRIC ARC AIR HEATER EMPLOYING A STRONG MAGNETIC FIELD AND COPPER ELECTRODES

By Robert F. Mayo, William L. Wells,
and Milton A. Wallio

SUMMARY

A magnetically rotated direct-current electric arc air heater employing water-cooled copper electrodes capable of operation at high power and high pressure with negligible test stream contamination has been successfully developed. Considerable improvement in arc air heater stability characteristics and reduction of electrode erosion rates over those previously encountered in arc air heaters utilizing constricted arcs was obtained by employing an intense magnetic field. The developed heater, small in physical size, has exhibited excellent operating characteristics over the full range of conditions investigated to date: stagnation pressures to 74 atmospheres, electrode input powers to 1200 kilowatts, arc voltages to 470 volts, arc currents to 3,800 amperes, and magnetic field strengths to 28,500 gauss. Numerous 30-second runs have been made for airflow rates up to 0.318 pound per second and arc chamber pressures to 40 atmospheres, with resulting test stream enthalpies up to 3,000 Btu/lb. Conversion efficiencies to 55 percent were obtained when a 0.5-inch-diameter throat nozzle and toroid-type center electrode were used. Efficiencies up to 33 percent were obtained with a 0.2-inch-diameter throat nozzle and cup-shaped center electrode. The total electrode material lost over 100 test runs utilizing the same arc heater components indicated that the test stream contamination was less than 0.1 percent.

INTRODUCTION

The need for facilities operating at stagnation pressures of the order of thousands of pounds per square inch and stagnation temperatures approximating $10,000^{\circ}$ R has aroused considerable interest in the use of electric arc type heating devices. Attention has been focused upon the high current arc operating within a pressure vessel through which a fluid test medium passes and is heated. Even though there have been advances in recent years in electric arcs near atmospheric pressure for various applications, there remains a substantial gap between the conditions of operation of these low-pressure arcs and those conditions obtainable with the high-pressure arc and the design knowledge associated therewith. Because of the extreme heating conditions encountered with high-pressure-arc operation, most early attempts employed uncooled consumable electrodes and arc chambers. However, severe problems with electrode erosion rates, arc stability, and test medium contamination result with this approach.

As part of an electric arc air heater development program at the Langley Research Center, an effort has been made to produce a low-contamination high-pressure-arc air heater for materials research. The program has led to the successful development of a magnetically rotated radial arc air heater employing water-cooled components. This heater utilizes a magnetic coil to produce field strengths on the order of 10,000 to 28,000 gauss to rotate the arc. This field strength is considerably above those previously used for this purpose.

The purpose of this report is to discuss the basic design concepts, describe the heater and equipment, and to present the heater characteristics over the normal operational range investigated (pressures to 600 pounds per square inch absolute, input powers to 900 kilowatts, and airflow rates to 0.318 pound per second). Additional characteristics are given based upon limited operation at pressures to 1,100 pounds per square inch absolute and input power to 1200 kilowatts. Also presented is relevant information developed during the design and operation of the heater and believed to be of substantial importance to designers of similar systems.

SYMBOLS

B	magnetic flux density, gauss
E	potential difference (between electrodes), volts
H	enthalpy, Btu/lb
I	current, amperes
M	Mach number
$\dot{m}$	airflow rate, lb/sec
P	pressure, atmospheres
$\overline{P}$	power, megawatts
T	temperature, ^{o}R
γ	ratio of specific heats

Subscript:

c	arc chamber

DESIGN CONCEPTS

Because of the limitations of arc heaters with uncooled electrodes, most present arc heater designs provide a magnetic field to force the arc to move over the electrode surfaces (ref. 1) and also provide water cooling for the electrodes. Movement of the arc over the electrodes is desirable not only to prevent quick destruction of the electrodes at a stationary arc spot but also to provide more uniform heating of the air.

For practical high-pressure application, however, other factors might tend to limit the value of moving the arc. In particular, contraction of the arc diameter (with corresponding increased erosion of the electrodes and increased radiation losses) might occur, since it has been reported that blowing cold air over a stationary arc can cause such a contraction (ref. 2), probably because of thermal conduction from the arc to the surrounding air (ref. 3). It was believed, however, that if the arc could be moved around an annular "racetrack" so rapidly that the period of one revolution was comparable to the ionization decay time, the arc would always move in a path of ionized gas and contraction of the arc might thus be avoided.

It was reasoned that this high rotational frequency for the arc could best be achieved with small diameter, concentric electrodes and with an especially strong magnetic field. Small-diameter electrodes provide a short path for one revolution of the arc and also make it possible to build a solenoid of small inside diameter - and thus with a high field strength - around the heater. Reference 4 discusses how a relatively low magnetic field applied perpendicular to the electric field can, at subatmospheric pressures, influence the current carriers in such a manner as to result in a totally diffused (disk-type) arc. Similarly, it was reasoned that the presence of a very strong magnetic field might, of itself, be useful in preventing the formation of a highly constricted arc even for operation at high pressure.

DESCRIPTION OF HEATER AND EQUIPMENT

The arc air heater comprised the following major components: arc chamber, electrodes, nozzle, magnetic coil, power supply, cooling water supply, and air supply. This section presents detailed descriptions of these components along with a description of the instrumentation and photographic equipment employed in the operation and evaluation of this arc heater system. A cross-sectional view, a photograph, and a block schematic diagram of the arc air heater and associated equipment developed under this program are shown as figures 1, 2, and 3, respectively.

Arc Chamber and Electrodes

The arc air heater pressure vessel is formed by a cylindrical copper barrel which also serves as the outer electrode. The nozzle and the center electrode feed-through housing form end closures for the barrel, as shown in figure 1. The

barrel, constructed of oxygen-free high-conductivity copper, is approximately 6 inches long with an inside diameter of $3\frac{3}{8}$ inches and a total wall thickness of about 7/16 inch. Two pressure vessels were used, differing only in the method by which cooling channels were provided. Figure 4 shows the first vessel, in which two lengths of 3/8-inch-diameter copper tubing were securely brazed in double-pitch helical semicircular grooves machined in the outside surface of the barrel to provide cooling. Figure 5 shows the second pressure vessel, in which helical grooves were machined into the barrel and covered with a sleeve to form internal cooling passages. For the initial operation, this arc heater employed a protective snugly fitting cylindrical carbon liner fitted in the copper barrel. The thickness of this carbon liner was incrementally decreased in successive tests until it was established that the water-cooled copper pressure vessel (electrode) was itself capable of withstanding all contemplated thermal and pressure loads.

The center electrode is made cup-shaped (figs. 1 and 6) in order to prevent arc attachment near the downstream center line. Figure 7 clearly shows the problem presented by arc attachment at the center of the downstream end where little electrode surface is utilized to accommodate the high heat loads. The "cup-shape" electrode has a minimum copper wall thickness of 1/16 inch and is water cooled. A range of arc gaps was studied by means of a series of electrodes with different outside diameters.

A second type of center electrode, a water-cooled copper toroid as shown in figure 8, is utilized for some operating conditions to bypass a portion of the airflow around the arc discharge area. This configuration permits stable arc operation with relatively high air mass flows and also allows fairly low temperatures, of the order of 2000° to 4000° R, to be obtained and the lower limits of test environments are thereby extended below those obtainable with the cup-shape electrode. To prevent arc attachment on the toroid support spokes, these spokes are angled upstream at 45° to 60° from the electrode center line as shown in figure 8. The toroid and spokes are fabricated of 5/8-inch-outside-diameter copper tubing with a wall thickness of 3/32 inch. Again, the arc gap between the electrodes may be varied by employing center electrodes of different outside diameters.

The axial positioning of the center electrodes within the chamber is accomplished as shown in figure 1 by an electrode positioning ring securely brazed on the electrode support tube as shown in figure 6(b). Pressure seal and electrical insulation are achieved as shown in figure 1. The inner electrical insulator is made of boron nitride. The outer pressure seal and insulator is made of bakelite.

Airflow is introduced into the arc chamber through two inlet tubes located in the end of the chamber as shown in figure 1. The inlets are oriented such that the air enters with a tangential velocity opposite to the arc rotation, in order to counteract partly the airstream rotation induced by the arc air drag. In addition, the air entrance ports are so located as to provide air cooling for the boron nitride inner insulator.

Nozzles

Two water-cooled copper nozzles were employed with excellent results over the entire operational range investigated in obtaining the data reported herein: a nozzle for high-pressure arc heater operation (P_c = 200 to 1,000 pounds per square inch) having a 0.2-inch-diameter throat and an exit diameter of 0.5 inch, and a second nozzle for low-pressure heater operation (P_c = atmospheric to 200 pounds per square inch) having a 0.5-inch throat diameter and an exit diameter of 0.75 inch. Both nozzles were constructed of oxygen-free high-conductivity copper.

The high-pressure nozzle (nominal $M = 3.3$ for zero boundary layer, $\gamma = 1.24$, P_c = 600 pounds per square inch absolute, and an exit pressure of 1 atmosphere) has directed coolant channeling along the back surface of the inner nozzle cone as shown in figure 9(a). Grooves nominally 1/16 inch wide by 1/16 inch deep were machined longitudinally in the outer surface of the inside nozzle wall circumferentially spaced to form ribs of 1/16-inch width on a nozzle wall thickness of 1/16 inch. Upon assembly of this nozzle the ribs form a continuous support for the encircling copper nozzle block. The ribs and nozzle block are silver soldered together; this procedure effectively makes the nozzle of one-piece solid-copper construction with excellent thermal conduction to all four sides of the internal cooling water channels for maximum heat-transfer capability and it also provides adequate structural strength for high-temperature and high-pressure operation. A nozzle extension was fabricated for this high-pressure nozzle to increase its exit diameter to 1.0 inch and extend the nominal Mach number to 4.5. The assembled nozzle and extension are shown in figure 9(b). Figure 2 shows a mirror view of the nozzle with extension in place on the arc heater facility.

The low-pressure nozzle, since it is subjected to much less severe heating effects than the high-pressure nozzle, was provided simply with nondirected coolant flow along the smooth back surface of the nozzle wall. The nozzle wall thickness is 1/8 inch. Figure 10 is a photograph of this nozzle, which is designed for $M = 2$ at P_c = 160 pounds per square inch absolute and atmospheric exhaust.

Magnetic Coil

The magnetic coil employed in the initial operation of the arc air heater is shown in figures 1 and 11. It was formed by six separate layers of 5/16-inch-outside-diameter (0.032-inch wall thickness) copper tubing. The tubing was insulated with 6-mil-thick fiber-glass sleeving and wound on an aluminum drum $5\frac{1}{2}$ inches in diameter and approximately 8 inches in length. Cooling water to the coil was directed to each layer individually in a parallel flow system. Electrically, the six layers were connected in series with each other and with the arc. This series arrangement produces the maximum transverse magnetic field intensity for a given arc current. A protective surge resistor was installed across the coil as shown in figure 6 to prevent any large inductive voltages on arc shutdown. The maximum continuous current capability of this layer-type coil was 2,250 amperes, for which current it produced a magnetic field of 17,000 gauss.

Accidental overheating of this first layer coil by overcurrent necessitated construction of a second coil. The second coil, shown in figure 2, had the same

general dimensions as the first but incorporated a different winding pattern. In lieu of the longitudinal layer-type windings previously employed, 12 pancake-type windings of two equal length layers each in planes perpendicular to the axis of the magnetic coil were employed. In addition, one longitudinal layer within the coil bore formed by the pancake layers was added to increase the magnetic field intensity further. Electrically insulated (6-mil fiber-glass sleeving impregnated with epoxy resin) copper tubing of 5/16-inch outside diameter and 0.049-inch wall thickness was used in the pancake coil, which has a maximum continuous current capability of 3,400 amperes and produces a magnetic field of 25,500 gauss.

The pancake winding has a marked advantage over the layer winding. The much shorter length of tubing per pancake coil permits an appreciable increase in total coil cooling capability. In addition, the multiple pancake coils, located at discrete stations along the coil axis, may be employed to contour the flux field by a selective electrical hookup of the individual pancake layers.

The electrical resistances of the two complete coils are approximately as follows: the layer coil, 0.10 ohm; and the pancake coil, 0.08 ohm.

Power Supply

Direct-current power for operation of the arc air heater was supplied by 480 2-volt lead-acid storage batteries of 860 ampere-hours capacity. They were arranged in four series-connected 250-volt banks as shown in figures 3 and 12. A detailed description of the power supply characteristics is presented in a later section. Four power transfer switches are employed to connect in series from one to four of the 250-volt battery banks for either arc operation or battery charging. Adjustment of the current level for a given voltage level is accomplished by selective hookup of current adjusting resistors (shown in fig. 3). Each stack of six parallel resistors has a resistance of approximately 0.03 ohm.

The power supply is applied to the load by two high-speed circuit breakers (fig. 3). These breakers are rated at 3,000 amperes and 1,000 volts direct current with an adjustable overload trip-out set at 6,250 amperes. Because of the occurrence of system surge voltages as later discussed under "Special Problems," the circuit breaker in the grounded leg (left circuit breaker in fig. 3) was converted to function only as a contactor which was programed to open 140 milliseconds after interruption of the ungrounded circuit breaker.

Cooling Supply

Cooling water for the arc heater and magnetic coil was supplied by a "blow-down" system comprising four 7.5-cubic-foot bottles, shown in figure 13, of which two bottles serve as supply and two as receivers. Cooling water flow of approximately 80 gallons per minute at 315 pounds per square inch absolute was achieved with regulated air pressurization of the supply bottles. A back pressure of 65 pounds per square inch absolute was maintained to raise the boiling temperature of the water to about 300° F. A closed-loop coolant system was employed to minimize scale formation and the resulting degradation of the system heat-transfer capabilities. As coolant water temperatures in excess of 250° F were encountered,

no scale-inhibiting additives which might decompose were introduced into the system.

Air Control

The air test medium for the arc air heater was supplied from a 2,000-pound-per-square-inch-absolute bottle field. The pressure was reduced to 1,200 pounds per square inch absolute ahead of the air control console. A pressure regulating system controlled the arc-chamber operating pressure to preset values. Controls were provided for starting the airflow upon initiation of the arc. Pressure-measuring instrumentation, air-mass-flow orifices, and safety interlocks were also included.

Instrumentation

In evaluating the performance characteristics of the arc air heater, conventional instrumentation was employed for the most part for determinations of system pressures, temperatures, air and cooling water flow rates, enthalpy, voltages, and currents. Iron-constantan thermocouples were used for all temperature measurements in an air environment and chromel-alumel thermocouples were used for measuring temperatures within the cooling water channels. The air-mass-flow rate was determined by use of a sharp-edged orifice meter. The electrical transducers used to measure the pressures in this airflow system are nominally accurate to within 1 percent. The net error in flow quantities, however, may be as large as 5 percent but is probably consistent to much less than 5 percent. The arc-chamber operating pressure was measured at a tap located in the upstream end of the chamber. (See fig. 1.) The cooling water flow rates were measured by turbine-type flow transducers. For calibration of the system components, flow transducers were temporarily installed in the individual water cooling lines to each heater component. A flow transducer was permanently located in the main cooling water supply line to the heater. Electrical outputs from the pressure-sensing transducers, thermocouples, and flow transducers were recorded by a galvanometer-type data recorder.

Electrical inputs of voltage and current to both the arc discharge and magnetic coil were measured as shown in figure 3 by recording transducers. These voltages and currents were also measured independently by means of appropriate potentiometer circuits driving fast response elements in the galvanometer recorder. A water-cooled calorimeter (shown in fig. 14) was used as one instrument to determine the test stream enthalpy. The calorimeter was a double-walled brass tube with a length-to-inside-diameter ratio of 22 to 1. At the entrance end of the tube, radial holes connected a cold-dilution-air chamber to the inside of the tube. Cold air could flow through the radial holes into the heated gas stream to reduce its temperature to a value which was measurable by use of conventional thermocouples. The calorimeter could be connected directly to the heater nozzle and would allow the test stream to flow through the tube. The exit end of the calorimeter supported a platinum-platinum-rhodium thermocouple rake to measure the reduced test stream temperature.

Photography

Photographic techniques were employed in the study of arc characteristics. One technique utilized a high-speed, rotating-prism framing camera capable of about 7,800 frames per second with an equivalent frame exposure of approximately 43 microseconds for mirrored direct photography. A second method employed a slow-speed, 64 frames per second, framing camera coupled with a 0.1-microsecond Kerr cell shutter arrangement as shown in figure 15. The Kerr cell shutter was electronically triggered to operate at midexposure of each frame photographed by the camera, and essentially "stopped" the arc. For pictures of the arc operating under pressurized chamber conditions, a transparent plexiglass window with a boron nitride nozzle insert as shown in figure 16 was employed to replace the water-cooled nozzle. The plexiglass window was 1/2 inch thick and $3\frac{3}{8}$ inches in diameter and remained functionally transparent for the entire run duration. The boron nitride nozzle insert had an outside diameter of 1 inch and a throat diameter of 0.2 inch.

Photographs were made both in black and white and in color with excellent results.

PROCEDURE AND TESTS

Operating Procedure

Since the radial arc air heater employs no components that physically move during heater operation and since the heater operation is inherently stable, the procedure for initiating and controlling arc heater operation is simple. The desired arc operating pressure is controlled by a pressure regulator set prior to the test run. The desired input power, operating pressure, and nozzle throat size determine the air-mass-flow rate (and hence the type of center electrode to be used as discussed previously), the arc-gap spacing, the open-circuit voltage (in increments of 250 volts), and the number and hookup of the current adjusting resistors. The selection of proper values for these variables to yield the desired heater operating conditions was initially exploratory until sufficient experimental operational data were obtained to permit reasonably accurate prediction of these values.

Arc initiation upon closing of the main circuit breakers is achieved by either of two methods. The first method consisted of placing between the electrodes a few strands of steel wool, which are instantaneously vaporized by the current and produce a cloud of highly conductive gas easily able to initiate the arc discharge. An alternate method has been employed to eliminate the need of "shorting" the arc gap by incorporating a commercial high-frequency starter unit in the arc system circuit. For small arc gaps both methods work satisfactorily if there is no prepressurization of the arc chamber. The steel-wool method was used since the high-frequency unit required prohibitive voltages at the electrodes for the arc gaps normally employed.

The airflow to the arc heater, controlled by an electrical-pneumatic solenoid valve, is initiated by an electrical signal from the circuit breaker while closing.

For the data reported herein, the average test duration time is 30 seconds, many times that required for attainment of equilibrium conditions. The cooling water supply has limited the maximum test run duration to date to 50 seconds.

All test runs were conducted with the instrumentation operating prior to initiation of the arc, in order to afford complete time records of arc operation and thus to permit detailed analyses of the critical transient phases of arc initiation and extinguishment. All components of instrumentation were regularly calibrated to minimize instrument error.

Series operation of the magnetic coil with the arc discharge provides excellent self-regulation of the arc heater system. To duplicate a previously run test condition, it is necessary only to duplicate the physical conditions, providing the same state of charge exists in the battery power supply.

A check on the validity of determining the enthalpy of the test airstream as the difference between the input electrical power and the thermal energy loss to the heater cooling water was performed. The arc air heater was operated at atmospheric pressure with no airflow for a sufficient length of time to establish equilibrium thermal conditions. With appropriate corrections made for the cooling water density variation with temperature and hydraulic power input, agreement within 3 percent was obtained between the power input to the heater and the thermal energy gained by the coolant.

For the photographic studies of the arc discharge phenomena under both atmospheric and pressurized chamber conditions, a front surface mirror was mounted downstream of the arc heater on the heater axial center line as shown schematically in figure 15. For tests at atmospheric chamber pressure, the arc heater was operated without a nozzle. The run duration was from 3 to 4 seconds for these atmospheric tests. For the high-pressure case the run duration was limited by the plexiglass window to about 0.7 second. Equilibrium pressure conditions in the arc chamber were achieved in less than 0.25 second by installing a prepressurized tank in the air line near the heater.

Range of Tests

One set of tests was made to determine the characteristics of the arc air heater with the cup-shape center electrode and the 0.2-inch-throat water-cooled nozzle. These tests covered a range of input powers from 350 kilowatts to 900 kilowatts and pressures up to 600 pounds per square inch absolute in increments of 100 pounds per square inch. For a number of short runs, arc input powers up to 1200 kilowatts were achieved. The current in these tests ranged from 1,100 amperes to 3,150 amperes. The highest arc chamber pressure was 1,100 pounds per square inch absolute and the highest arc voltage was 470 volts. The tests made to determine characteristics of the arc air heater with the $2\frac{1}{2}$-inch-diameter toroid electrode and the 0.5-inch-throat water-cooled nozzle covered a range of input powers from about 350 kilowatts to 750 kilowatts. A toroid electrode of

$2\frac{3}{4}$- inch overall diameter was also used with this nozzle for test runs in which the airstream exit temperature was below 3500° R. Operation of the heater with this nozzle was with pressures of 130 pounds per square inch absolute to 180 pounds per square inch absolute.

Air-mass-flow rates of 0.025 pound per second to 0.218 pound per second were used with the high-pressure nozzle. Flow rates used with the low-pressure, larger throat nozzle ranged from 0.170 pound per second to 0.318 pound per second. Magnetic field strengths, depending on the arc current, ranged up to 23,600 gauss; and some short test runs made for the purpose of studying arc phenomena field strengths up to 28,500 gauss, with arc currents up to 3,800 amperes, were obtained. Since such high currents exceeded the continuous rating of the magnetic coil and supply system, the permissible periods of operation were determined by the "heat-sink" capability of the magnetic coil, which allowed about 1 second of operation at stable conditions. During the development program arc gaps from 1/32 inch to $1\frac{3}{16}$ inches were used.

RESULTS AND DISCUSSION

Power Supply Characteristics

The electrical characteristics of the battery power supply are shown in figure 17 as curves of voltage and power against load current. The power supply has a maximum power output of 1.62 megawatts, occurring at a load current of about 3,400 amperes. This peak power output remains essentially constant for approximately the first 20 seconds and then decreases fairly rapidly. It is interesting to note that this peak output power condition occurs when the battery output voltage is approximately one-half the open circuit voltage. At this point the arc impedance and the external circuit impedance are essentially equal as would be expected. This battery voltage drop serves to replace a large portion of the external ballast resistors normally required in arc heater system circuits. At the maximum power level, little or no external ballast is required for stable arc heater operation.

Operating Characteristics

Arc startup and response.- The starting characteristics of the arc air heater are shown in figure 18, a portion of a typical test run record obtained from a fast-response galvanometer recorder. Both the arc voltage and the arc current attain steady-state values for the existing pressure very quickly, since the time constant of the electrical system is only about 0.005 second. Accordingly, the starting characteristics shown in figure 18 are essentially determined by the starting characteristics of the airflow system. The electrical-pneumatic solenoid valve controlling the air mass flow is actuated to initiate airflow by the same signal that actuates circuit breaker closing. As shown in figure 18, there exists in the airflow system a lag of approximately 0.2 second before any significant chamber pressure rise is noted, because of the slow control valve response.

When the airflow is introduced into the arc chamber and is heated, a rapid increase in chamber pressure is obtained. The desired equilibrium run pressure is shown to be achieved in less than 1 second. Equilibrium pressure in the arc chamber was achieved in about 0.25 second for those runs in which photographic studies were made. This faster response was achieved by adding a prepressurized tank to the air line just upstream of the heater, as mentioned previously.

The center electrode coolant temperature, as shown in figure 18, also follows the buildup of chamber pressure very closely and attains an equilibrium level in about 1 second. The cooling water temperature for the outer electrode or arc chamber barrel is not indicated in figure 18; it required approximately 4 seconds to attain a constant value, because of the increased wall thickness and longer coolant passage lengths.

The exhaust gas enthalpy (not shown), as determined by the external heat-exchange calorimeter previously described, follows very closely the time buildup history of the center electrode coolant temperature. Thus, equilibrium operation of the arc air heater, producing an exhaust gas stream with steady characteristics, is achieved in approximately 1 second.

Although figure 18 shows only the first 4 seconds of a typical test run, nearly constant equilibrium conditions are maintained for the duration of the run without any additional external regulation. Series operation of the arc and magnetic field coil provides circuit self-compensation for small circuit disturbances. That is, any reduction in current results in a decreased value of B which, in turn, allows an increase in current because of the reduction in voltage drop across the arc.

Figure 19 shows the arc air heater in operation at a chamber pressure of 600 pounds per square inch, a power input to the electrodes of 944 kilowatts, and an airflow rate of 0.102 pound per second. The heated airstream is shown exhausting through the nozzle with the 0.2-inch-diameter throat.

Arc voltage-current-pressure relationship.- The relationship between arc voltage (voltage across the electrodes), current, and chamber pressure is shown in figure 20 for an arc gap of 7/16 inch and a ratio of magnetic flux density to current B/I of 7.5 gauss/ampere. Each curve represents operation at a constant chamber pressure as indicated and with the 0.2-inch-diameter throat nozzle and cup-shaped center electrode. Most of the curves show that an increasing current results in a slightly higher arc voltage; as a result, a slightly positive effective coefficient of resistivity $\left(\text{defined as a positive slope of the } \frac{dE}{dI} \text{ curve}\right)$ is indicated for the arc. The desired operating current for a given pressure was obtained by adjusting the series ballast resistors.

In figure 21 the arc voltage is shown as a function of arc chamber pressure for an arc current of 1,750 amperes. (This current represents an approximate average current for all of the curves in fig. 20.) The fairly sharp rise in arc voltage with increasing arc chamber pressure in the lower pressure region (up to about 400 pounds per square inch absolute) is basically the normal anticipated voltage rise with increasing pressure. However, at higher arc chamber pressures (400 pounds per square inch absolute and greater), this sensitivity of arc voltage

to increasing pressure is rapidly diminished. At higher pressures the back electromotive force generated by the arc is reduced because the higher air drag on the arc lowers the arc rotational speed.

Air enthalpy and temperature.- To show the relationship between arc input power, operating pressure, and the enthalpy of the air leaving the supersonic nozzle, it was found convenient to introduce the ratio of air mass flow (pound/second) to input arc power (megawatts). To aid the reader in determining the actual values of input power and air-mass-flow rate used in preparing the following graphs that use this parameter, figure 22 shows the conditions of operation at which the test runs were made. The corresponding values of air-mass-flow rates are obtained by taking the product of the abscissa and the ordinate (after changing the ordinate from kilowatts to megawatts).

The enthalpy of the air leaving the supersonic nozzle, as determined by the energy balance of the arc air heater, is shown in figure 23. The five hyperbolas shown are contours of constant efficiency and the shaded areas cover the experimental results. The range of experimental efficiencies can be readily seen from the location of the shaded areas relative to the contours. The 0.5-inch-diameter throat nozzle curve is for operating pressures of 140 to 180 pounds per square inch absolute. The 0.2-inch-diameter throat nozzle curve is for operating pressures of 100 to 930 pounds per square inch absolute. It is of interest to note that the arc air heater with the 0.5-inch-diameter throat nozzle and toroid center electrode operates with an efficiency substantially greater than the heater with the 0.2-inch-diameter throat nozzle and cup-shape center electrode. This is considered to be the effect of a higher air velocity in the arc chamber which results in a shorter residence time and a decrease in arc-induced rotation of the heated air. (The long residence time and high rotational velocities of the heated air tend to increase conductive and convective heat losses to the walls.) Figure 23 also gives an indication of the efficiency required to achieve a given enthalpy of the air entering the heater at 520° R (H = 130 Btu/lb). Operation with the 0.5-inch-diameter throat nozzle and toroid center electrode results in about 55-percent efficiency over the range investigated. Operation with the 0.2-inch-diameter throat nozzle and the cup-shape center electrode results in a 15- to 33-percent efficiency over the range investigated, the lower efficiencies being for the lower pressures and the higher efficiencies being for the higher pressures (and correspondingly higher airflow rates). When the jet was operated without a nozzle (atmospheric pressure) efficiencies up to 80 percent were obtained. Although arc-induced rotation of the heated air in the chamber is probably enough to affect adversely the operating efficiency, the rotation of the air as it leaves the nozzle exit is considered to be very small for the 0.5- and 0.2-inch-diameter throat supersonic nozzles. However, when the jet is operated without a nozzle (nearly equivalent to a 3-inch-diameter subsonic nozzle operating at atmospheric pressure where the arc rotation is greatest), rotation of the exaust air is definitely detectable and most of the air is concentrated near the outer diameter of the barrel.

The gas temperatures corresponding to the enthalpy values in figure 23 were determined by use of a Mollier enthalpy chart such as reference 5 and are shown in figure 24. In this temperature plot there is increased separation of the different constant-pressure curves for the same gas enthalpy since for a given enthalpy the higher pressure air has the higher temperature. The data points

through which the curves were faired in figure 24 (for operation with the 0.2-inch-diameter nozzle) have been omitted in order to show more clearly the trends in temperature variation. These data are shown in table I.

TABLE I.- HEATER AIR STAGNATION TEMPERATURE WITH INCREASING $\frac{\dot{m}}{P}$ FOR OPERATION AT DIFFERENT STAGNATION PRESSURES

$\frac{\dot{m}}{P}$, lb/sec / megawatt	T, °R	P_c, lb/sq in. abs.	$\frac{\dot{m}}{P}$, lb/sec / megawatt	T, °R	P_c, lb/sq in. abs.	$\frac{\dot{m}}{P}$, lb/sec / megawatt	T, °R	P_c, lb/sq in. abs.
0.062	7295	195	0.113	5640	396	0.123	6135	595
.077	6855	200	.116	6290	401	.140	4965	591
.100	5465	203	.129	5600	396	.142	5725	593
			.132	5620	386	.146	6885	608
.096	6730	396	.133	5760	406	.155	6705	598
.102	6380	395				.175	5625	602
.103	6310	385	.107	6705	590	.223	4195	599
.104	6210	398	.108	6665	578			
.112	5570	387	.108	6205	585	.185	5700	930
.112	6465	394	.122	6904	606			

The values of air enthalpy and temperature presented in figures 23 and 24 were obtained from an energy balance for the heater for each run. In this method the energy added to the system is determined by measuring the electrical power input and the energy gained by the air is assumed to be that portion of the input energy that is not lost to the cooling system. Because of the large cooling water flow rates and relatively low temperature rise, a small error in determining the original data can result in a relatively large error in the final values of air enthalpy and temperature. As a check on the arc air heater energy balance method, an additional method was temporarily used as mentioned previously. This method made use of a calorimeter connected to the heater as shown in figure 14. Cold dilution air was introduced into the heated airstream in sufficient quantity to allow the temperature of the mixture to be measured with thermocouples. The measured heat gained by the total airflow and by the water that cooled the calorimeter walls was then related back to the enthalpy gained by the air leaving the sonic nozzle. A comparison of the results obtained by the two methods is shown in figure 25. The points on this graph, which were obtained from the calorimeter method, agree very well with the curve which represents an average of the enthalpy values obtained from the heater energy balance method. In these comparison tests, which were made early in the development program, a sonic ceramic-lined nozzle was used. These test points are not included in the basic data indicated in figure 22, since these data represent operation with all water-cooled metallic components.

A comparison of the present data (obtained with the water-cooled metallic nozzle) with the values of chart 21 in reference 6, which show enthalpy as a function of stagnation pressure and air mass flow per unit of nozzle throat area, was made for a select number of runs. Correlation for the lower pressure runs made with the 0.2-inch-diameter throat nozzle was not good. In some cases the enthalpy as determined by the heat balance of the arc air heater is only 50 percent of that

as determined by the reference chart. In the high-pressure runs the agreement was considerably closer. At the highest pressure (930 pounds per square inch absolute), agreement was within less than 10 percent. The reasons for the large disagreement at the lower pressures and with the 0.2-inch-diameter throat are not yet fully understood, although it is apparent that both the air swirl and boundary-layer effects would be greater for the lower pressure case.

Energy and cooling distribution.- The energy distribution (or heat balance) for a typical arc air heater test run at a power input of 680 kilowatts (672 Btu/sec) and an arc chamber pressure of 598 pounds per square inch absolute is shown in figure 26. In addition are shown the cooling water flow rates to the individual heater components. As would be anticipated, the outer electrode or arc chamber barrel absorbs most of the arc input energy, about 47 percent. Absorbing lesser amounts are the center electrode (15 percent) and the water-cooled nozzle (6 percent). Of the total input energy to the arc for the run illustrated, approximately 32 percent remains with the air at exit from the nozzle. Since the operating efficiency is not the same at all operating conditions (see fig. 23), it is apparent that this energy distribution also varies with operating conditions.

The maximum heat loads imposed on the arc air heater with all water-cooled copper components are as follows: outer electrode and pressure vessel, 490 Btu/sec; center electrode, 250 Btu/sec; nozzle (Mach number ≈ 4.3), 88 Btu/sec. These values do not correspond to a particular test run but are the maximum values encountered during the entire test program.

Electrode erosion.- Operational data obtained over a large number of test runs of the arc air heater show that the electrode erosion rates in this heater are higher for the cathode than for the anode. The choice of the outer electrode to function as the cathode was based on this fact, since the outer electrode had the greater area and wall thickness. An accurate determination of the loss rate is difficult because of the small amount of material lost relative to the weight of the electrodes.

For a block of 180 test runs, the ratio of total electrode weight loss to total airflow indicated that the average airstream contamination by eroded copper is less than 0.1 percent. Approximately 610 pounds of air were used for the cited 180 runs. Copper loss from the electrodes, based upon dimension changes of the electrodes, was approximately 0.3 pound.

Arc Rotation and Diffusion

Considerable attention was directed toward the nature of the arc itself. Initial tests indicated a mode of arc operation that was appreciably different from that known to exist in other arc heaters operating in the same current and pressure ranges. One possible indication of some arc diffusion was the absence of arc "tracking" on the electrodes after operation with d-c currents up to 3,800 amperes. Essentially identical heat losses to the center electrode, whether used as the anode or cathode, indicated a deviation from constricted-arc operation. The current, voltage, and pressure relationships further indicated a different type of arc operation from that observed in earlier work.

The first photographic arc study utilized a high-speed rotating prism camera. This camera operated at about 7,800 frames per second with an equivalent exposure time of 43 microseconds. In photographs taken with this arrangement, the arc appeared as a continuous 360° annulus when relatively high currents and magnetic fields were used. Such a photograph is shown in figure 27 for which the nozzle was replaced by a transparent window with a ceramic nozzle insert. (See fig. 16.) The photograph in figure 27 was taken at the following operating conditions: $I = 2,600$ amperes, B above 19,500 gauss, $P_c = 35$ pounds per square inch absolute. For operation at much lower currents and magnetic fields, the arc illuminated only about half of the annulus for the same exposure time. Figure 28 shows a typical photograph for operation at the conditions: $I = 1,200$ amperes, $B = 9,000$ gauss, and $P_c = 1$ atmosphere. From the study of many photographs of this type taken at various conditions, a general knowledge of the arc speed was obtained. From this photographic study alone, however, it remained uncertain as to whether the arc was of a highly constricted nature, rotating at a high velocity or was somewhat diffused and moving more slowly.

The second method of photographic arc study made use of a framing camera and Kerr cell shutter arrangement to permit an exposure time of only 0.1 microsecond. A schematic diagram of this arrangment is shown in figure 15 and is explained in the "Description of Heater and Equipment" section of this report. The system was checked for proper operation by use of cathode ray oscilloscopes. Photographs showed that the Kerr cell shutter transmitted a small amount of "leakage" light during the time that the mechanical shutter of the camera was open. During this time the arc made many revolutions, which resulted in a slight exposure of the film showing the arc annulus between the electrodes. The exposure times involved are such that the superimposed 0.1-microsecond exposure contributes about 70 percent of the total light. Since the leakage light is distributed evenly around the entire image of the arc annulus and the 0.1-microsecond exposure only over the instantaneous image of the arc, the resulting definition is very good.

Figure 29 shows some of the many views obtained of the arc discharge for the corresponding operating conditions noted. These photographs were taken with the Kerr cell system. As shown, the arc appears to manifest itself in many configurations. In some of the frames the discharge appears to be almost completely diffused. In others, the discharge appears almost invisible, although with continuous current flow it certainly exists. Still other frames show only small fragments of arc filaments while some show a general broad "cloud" type discharge.

It was concluded that the photographic images represented an actual arc discharge rather than vaporized electrode material (often referred to as plasma jets in other literature) with an embedded constricted arc. This conclusion was partially based upon the following argument. From the high-speed photographs taken at near atmospheric pressure and high values of current and magnetic field, the average arc speed around the electrode has been determined to be greater than 9×10^5 centimeters per second. If a highly constricted arc is assumed, this value would be even greater. The speed of vaporized material across the annulus would hardly exceed 5×10^4 centimeters per second. (See ref. 2.) Under these conditions, this "plasma jet" could cover only about 20 percent of the distance between the electrodes during the time required for the arc to move into an adjacent area $\left(\text{say, } 2\frac{1}{2}^\circ \text{ away}\right)$. Therefore, an instantaneous picture should show a

constricted arc midsection with the plasma jets trailing outward toward the center of the arc gap. To date, such an image has not been obtained under normal steady-state operating conditions.

For atmospheric-pressure conditions it was noted that the arc moves around the annulus with rotation of frequencies (or speeds) on the order of 20,000 revolutions per second, depending upon the exact current and magnetic field. For the lowest current range studies, about 1,100 amperes, the rotational frequency was about 10,000 revolutions per second. The rotation or speed at the highest current studied, 3,800 amperes and 28,500 gauss, has not been determined since a complete 360° rotation is experienced during a 43-microsecond exposure time. In fact, a complete rotation of the arc is experienced during the same exposure time, for conditions of 2,500 amperes and 18,500 gauss.

Photographs were also taken under normal operating conditions, including pressures up to 600 pounds per square inch absolute, by use of the transparent window arrangement mentioned earlier. Two typical frames of 43-microsecond exposure time are shown in figure 30 where the arc is operating with a chamber pressure of 600 pounds per square inch absolute. Although it is very difficult to determine the arc rotational speed from such photographs, it is apparent that the speed is much less than the speeds found at atmospheric pressure. From studies of original negatives, which are somewhat clearer than the prints, the arc rotational frequency appears to be on the order of 2,000 revolutions per second or less, depending upon current and magnetic field values. Light output from the arc was sufficiently decreased at high pressures to necessitate use of a larger lens aperture on the camera.

Some photographs taken at high-pressure conditions with the Kerr cell shutter arrangement are shown in figure 31. These photographs were taken when the arc chamber pressure was about 600 pounds per square inch absolute and, in most cases, the arc current was 1,800 amperes as indicated. The dark radial lines seen in these photographs are due to cracking of the plexiglass windows at high pressure. Information gained from this type of photograph indicates that the arc discharge has even less definition at the higher pressures. In fact, at the 600 pounds per square inch absolute level it appears, most of the time, to maintain itself in a highly diffused state.

Of considerable interest is the fact that for each run with pressurized conditions there was definitely one, and probably two, periods in which photographs show what appears to be a uniform complete diffusion of the arc discharge. These conditions exist during the periods of increased B to I ratio, which occurred when there was a transient decrease in arc current. For a better understanding of this phenomenon it is necessary to consider the arc starting and stopping process. The arc starts at atmospheric pressure and then the chamber pressure is allowed to rise quickly to the desired run value. The initial arc current rises to some high value and then decreases to its run value as the increased chamber pressure causes an increase in arc voltage. Since the arc and magnetic coil are electrically connected in series, the magnetic flux follows this same pattern. However, as the arc current begins to decrease eddy currents in the copper chamber (and possibly eddy currents in the plasma) tend to hold the enclosed magnetic flux up to its higher value. That is, the flux lags the current, which for a short time produces a higher B to I ratio. Again at arc shutdown, the copper

chamber (and plasma) tends to hold the enclosed magnetic flux up to its normal run value as the arc current begins to decrease. Photographs such as those of figure 31 concluded (0.1 μsec exposure) indicate a completely diffused arc (360° disk) for each run during arc termination. This phenomenon is also shown on pressure buildup for many runs. Since the sampling rate of the Kerr cell system is only 64 per second, the effect could very well have been missed on the runs for which it was not observed.

The question remains as to whether the apparent complete diffusion of the arc during each case of decreasing current is due solely to the change in the B to I ratio. If so, there appears to be a possible steady-state operation with this type of arc discharge with a greater B to I ratio than that used at present (B/I = 7.5 gauss/amp). Some insight as to the required ratio may be gained from studies of the current decay upon pressure buildup. Results of such studies indicate that the increase of the B/I ratio could not have been more than 50 percent. On arc shutdown this ratio could be considerably higher since the current decays very rapidly. Further research will be required to determine whether the B to I ratio is the most important single factor in producing steady-state operation with a completely diffused arc.

Special Problems

Operation of the magnetically rotated radial arc air heater revealed several areas in which problems were encountered or strongly indicated. Some of these problems are considered to be of sufficient importance in the design and operation of arc air heaters of this type that an awareness of them is essential.

Voltage surge.- During the early phases of the development program of the arc air heater a single circuit breaker was employed in the electrical supply system to prevent circuit overload and to furnish circuit interruption. After this breaker failed two breakers were installed, one on each leg of the electrical circuit (as shown in fig. 6), and the system was grounded at the heater outer electrode. The breakers were operated simultaneously to close and open the circuit as recommended by the breaker manufacturer. However, breaker failure again was experienced upon a normal run termination. Both breakers were involved in this failure.

After the breakers were repaired, a number of tests were made in an effort to determine the exact cause of the failures. The investigation included an effort to determine whether high voltages were being created on arc heater shutdown. The tests failed to indicate any excessively high voltages from the external inductance during current decay. Protection was already afforded against development of excessive voltages by the magnetic coil by use of the surge resistor across the coil. This left for consideration only the arc heater decay conditions.

The rotating plasma in the arc air heater has an "equivalent capacitance" (ref. 7, pp. 430-435) that is a function of its physical state and the transverse magnetic field. A change in the equivalent capacitance of the rotating plasma system will occur with the decaying magnetic field and changing arc plasma conditions. The capacitive values between the supply circuit, ground, and arc heater

are sufficiently small that relatively high voltages could be generated by a small amount of charge. Thus, it seemed conceivable that a surge voltage might be produced under certain conditions of circuit decay.

Both cases of cited breaker failure occurred while operating with atmospheric chamber pressure, relatively small airflow rates, and high power conditions. These conditions represent the case when the plasma temperatures and rotational speeds are at their maximum values experienced with this system.

A number of test runs, employing cathode ray oscilloscopes displaying the system voltages, were conducted to determine the possibility of a surge voltage occurring under the range of normal arc air heater operation. Approximately 25 test runs were conducted without observance of an abnormally high surge voltage being developed by the arc air heater upon arc shutdown. However, the tests do not exclude the possibility of a surge voltage being created since terminal conditions of circuit decay are approached with varying rates even for equivalent run conditions. This condition occurs because of vastly different extinction times and the varying arc and plasma conditions that can exist while nearing the minimum current level at which the arc will maintain itself. Tests did indicate, however, that less severe voltage fluctuations resulted on arc shutdown from interrupting only the circuit breaker on the ungrounded side, and leaving the outer electrode of the heater connected to the power supply.

In an effort to avoid additional breaker failures, the circuit was arranged so that the breaker in the ungrounded side was set to interrupt prior to operation of the breaker in the grounded side. The delay between operation of the two breakers was set for about 140 milliseconds which was considered to be of sufficient length to allow decay of the plasma state and magnetic field. Furthermore, the breaker in the grounded side of the circuit was altered so that it acts as a contactor and thus a possible tripping of this breaker due to any overload is avoided. This arrangement allows the heater to remain connected to the power supply through the grounded side of the circuit during arc shutdown. The second breaker, or contactor, furnishes circuit interruption in the event of failure of the first breaker.

Arc transfer.- It is desirable to minimize the distance between the center electrode and the nozzle throat in order to reduce both the radiation losses and the convective losses from the hot gas to the cool chamber wall. There exists some minimum distance at which the center electrode may be spaced from the nozzle for this type of heater configuration. This distance limitation results from two types of arc transfer that can occur when the nozzle is constructed of an electrically conducting material.

The first type is simply a physical transfer of the arc to a downstream location, where it would extend between the center electrode and the nozzle, at some acute angle to the heater axis and to the magnetic field. The magnetic field has a maximum effect on the arc when it is normal to the arc; accordingly, this type of arc transfer has the effect of a reduction in magnetic-field value. Of course, this type of arc transfer could be eliminated simply by insulating the conducting nozzle from the outer electrode.

A second type of arc transfer can occur even if the nozzle is insulated from the remainder of the arc air heater. Instead of traversing the arc gap normal to the magnetic-field lines, the arc current may follow a path of higher conductivity from the center electrode along the magnetic-field lines downstream through the plasma and into the nozzle surface. The current can then flow across the dense nozzle material, where the magnetic field has little effect, and then reenter the plasma near the outer electrode wall. From there the current can follow the magnetic-field lines upstream and into the outer electrode surface. Reference 7 (pp. 459-462) explains this effect more thoroughly as related to the neutralization of space charges between electrodes.

To avoid arc transfer in the heater configuration reported herein, the center electrode was located about four arc gap lengths upstream of the beginning of the nozzle. This position also falls slightly upstream of the maximum magnetic flux density point. If the center electrode was moved closer to the nozzle, bright spots were observed on the nozzle surface after a run. The bright spots are thought to be caused by short-duration constricted discharges to the nozzle. Examination of the nozzle after one such run showed about 10 spots per square inch of surface. No runs were made with the center electrode positioned close enough to the nozzle to allow a complete arc transfer.

Both of these arc-transfer problems can theoretically be eliminated by properly contouring the magnetic-field lines to parallel the nozzle contour. With this arrangement, the nozzle convergent cone can act as the outer electrode.

Transient characteristics.- The major variations in the ratio of magnetic flux density to arc current B/I occur at arc startup and arc shutdown. During these periods of changing current the mutual inductance between the coil and copper pressure vessel is such that the magnetic flux appreciably lags the current. If the coil is wound on a continuous aluminum drum, the magnetic flux will lag the current even more because of the increased mutual inductance. Figure 32 shows the results of calculations made to estimate the transient response based upon a similar idealized system. The effects of a varying arc chamber pressure are not considered in this plot.

It has been pointed out that for reduced electrode erosion, maintenance of a high value of the B/I ratio is desirable. The following example is given as experimental evidence of the effects of the previously mentioned mutual inductance and the resulting effects of the B/I ratio. Because of accidental overheating of the original coil, a second coil was built. Because of the different design, the second coil produced (for a given current) a magnetic-field intensity that was about 8 percent less than that of the original coil. Initial operation with this new coil resulted in a drastic increase in electrode erosion. Removal of the continuous aluminum drum on which the coil was wound reduced the erosion somewhat. However, it was not until more turns were added to the inside diameter of the coil that the B/I ratio was brought up to about 7.5 gauss per ampere, and the erosion rate returned to its former low level. Prior to this experience, it was not known at what point the B/I ratio became critical for this geometry.

Maximum electrode erosion is considered to take place at arc startup for series operation of the coil and arc. However, since arc startup is of short duration, it appears that series operation is desirable because of other beneficial

effects. When the magnetic coil was excited by a separate power supply, tests revealed that where the arc current exceeded the coil current by about 12 percent, the arc current suddenly climbed much higher than the small planned increase. Under a decreasing B/I ratio, the arc impedance apparently decreases rapidly when the B/I ratio falls more than about 12 percent below the normal level of operation (7.5 gauss/ampere). As an example, one such run was made with separate excitation of the coil and arc. Circuit adjustments were made in expectation of getting 1,800 amperes in the coil and arc based on series operation. Upon arc initiation, however, the arc current climbed to about 5,000 amperes and dropped back to 4,100 amperes when the arc chamber pressure reached its preset value. The run was terminated after 2 seconds due to the excessive arc current. For stable operation, transients in the magnetic field and in the arc current should be about the same. In the present arc heater, series operation provides this desired nearly constant B/I ratio during a run. Small variations in B/I occur during the run due to fluctuations in the arc current. However, the circuit inductance tends to damp out the higher frequency arc current fluctuations (on the order of 200 cycles per second and up) whereas, the series operation, as already noted, tends to damp out arc current fluctuations below 200 cycles per second.

Small variations occur in arc voltage and current because of a number of events during a run. The shifting arc discharge attachment along the electrode surface, varying arc lengths, and varying conditions of the electrode surface, all have some effect. However, the net variations of current and voltage under normal operation appear to be less than 5 percent. Furthermore, these variations are of such high frequency that the exit flow conditions are not appreciably unsteady or irregular.

CONCLUSIONS

The investigation and operation of a magnetically rotated, radial electric arc air heater employing water-cooled copper electrodes and a battery power supply leads to the following conclusions:

1. A high value of transverse magnetic field (field set up by external magnetic coil) produced some diffusion rather than contraction of the arc discharge where the arc path was confined to a small annular volume. High-speed photographs indicated less contraction at 40 atmospheres pressure than at 1 atmosphere pressure.

2. Operation of the reported heater with a transverse magnetic flux density B to arc current I ratio of 7.5 gauss/ampere results in low electrode erosion (less than 0.1 percent of airflow by weight). A reduction of this ratio by about 8 percent results in increased erosion that is readily apparent by visual inspection.

3. In contrast to separate excitation of the arc and magnetic coil, series connection of the arc and coil maintains a near constant B/I ratio and results in stable operation of the heater.

4. For heater operation between about 6 and 40 atmospheres pressure where a nozzle with a 0.2-inch-diameter throat and a cup-shape center electrode was used, efficiencies ranged from 15 to 33 percent. Operation at the higher pressures tended to produce the higher efficiencies. Operation at about 10 atmospheres pressure using a nozzle with a 0.5-inch-diameter throat (with correspondingly higher airflow rates) and a toroid center electrode resulted in efficiencies of about 55 percent over a rather wide range of power inputs.

5. To date, for runs of 30-second duration, air enthalpy values of about 3,000 Btu/lb have been achieved when the 0.2-inch-diameter throat nozzle and cup-shape center electrode were used. Air enthalpy values up to 1,800 Btu/lb have been achieved with the 0.5-inch-diameter throat nozzle and toroid center electrode.

6. High-speed photographs indicated total diffusion of the arc (360° disk between the electrodes) during certain transient periods of operation. Further research will be required to determine whether an increase in the B/I ratio can produce this total diffusion as a steady-state condition and to determine the effect this condition might have on heater efficiency and electrode erosion.

Langley Research Center,
National Aeronautics and Space Administration,
Langley Station, Hampton, Va., August 27, 1963.

REFERENCES

1. John, Richard R., and Bade, William L.: Recent Advances in Electric Arc Plasma Generation Technology. ARS Jour., vol. 31, no. 1, Jan. 1961, pp. 4-17.

2. Finkelnburg, W., and Maecker, H.: Elektrische Bögen und thermisches Plasma. Handbuch d. Physik, Bd. XXII, Springer-Verlag, 1956, pp. 254-444.

3. Yankov, V. V.: Behavior of a High-Pressure Electric Arc. Soviet Physics - JETP, vol. 6, no. 11, May 1962, pp. 965-967.

4. Hess, R. V., Burlock, J., Sevier, J. R., and Brockman, P.: Theory and Experiments for the Role of Space-Charge in Plasma Acceleration. Electromagnetics and Fluid Dynamics of Gaseous Plasma, Vol. XI of Microwave Res. Inst. Symposia Ser., Polytechnic Press of Polytechnic Inst. of Brooklyn, c.1962, pp. 269-305.

5. Feldman, Saul: Hypersonic Gas Dynamic Charts for Equilibrium Air. AVCO Res. Lab., Jan. 1957.

6. Yoshikawa, Kenneth K., and Katzen, Elliott D.: Charts for Air-Flow Properties in Equilibrium and Frozen Flows in Hypervelocity Nozzles. NASA TN D-693, 1961.

7. Glasstone, Samuel, and Lovberg, Ralph H.: Controlled Thermonuclear Reactions. D. Van Nostrand Co., Inc., c.1960.

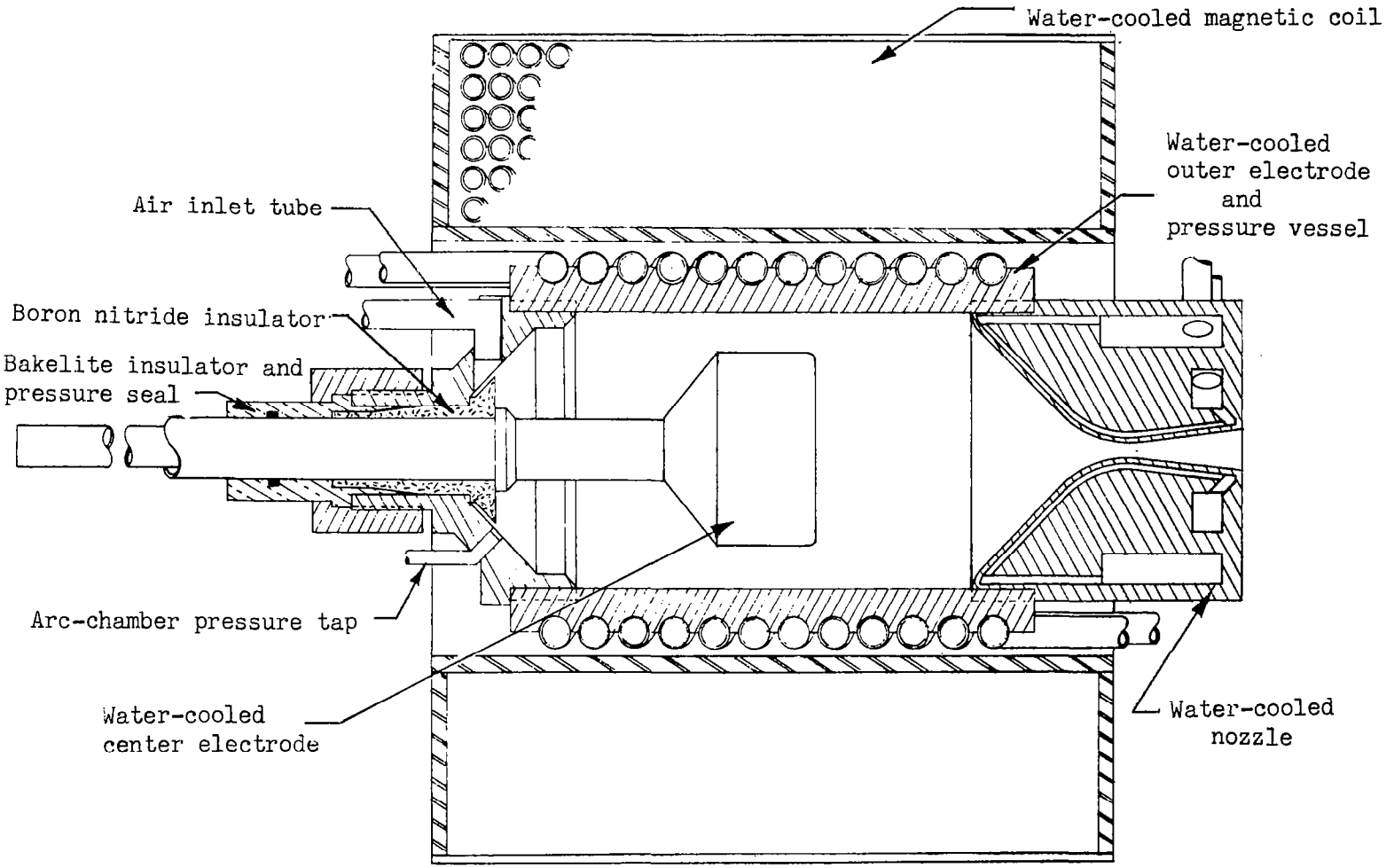

Figure 1.-.Cross-sectional view of magnetically rotated radial arc air heater.

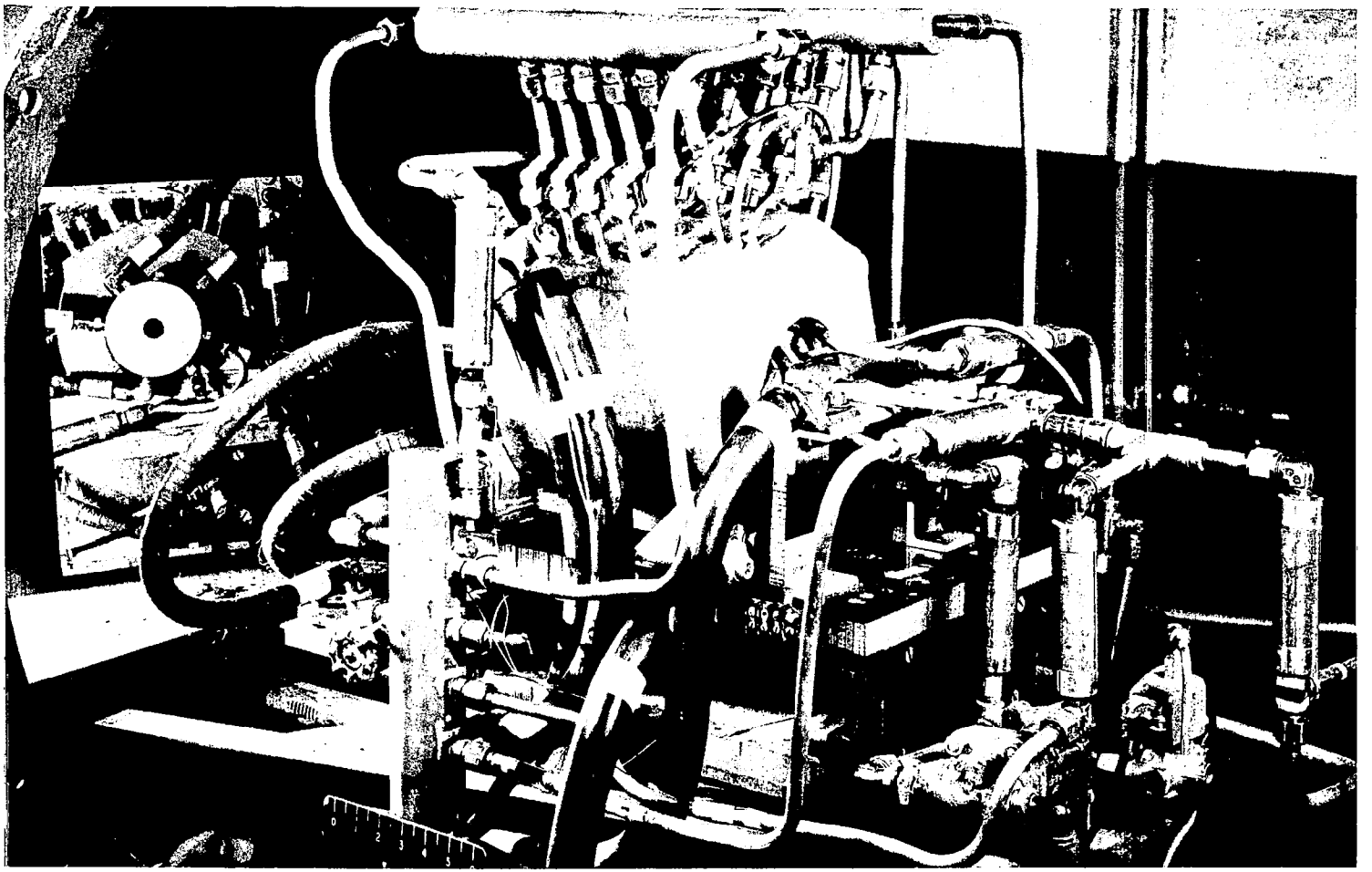

L-61-3755

Figure 2.- Arc air heater with pancake-type magnetic coil. Mirror shows nozzle end of heater.

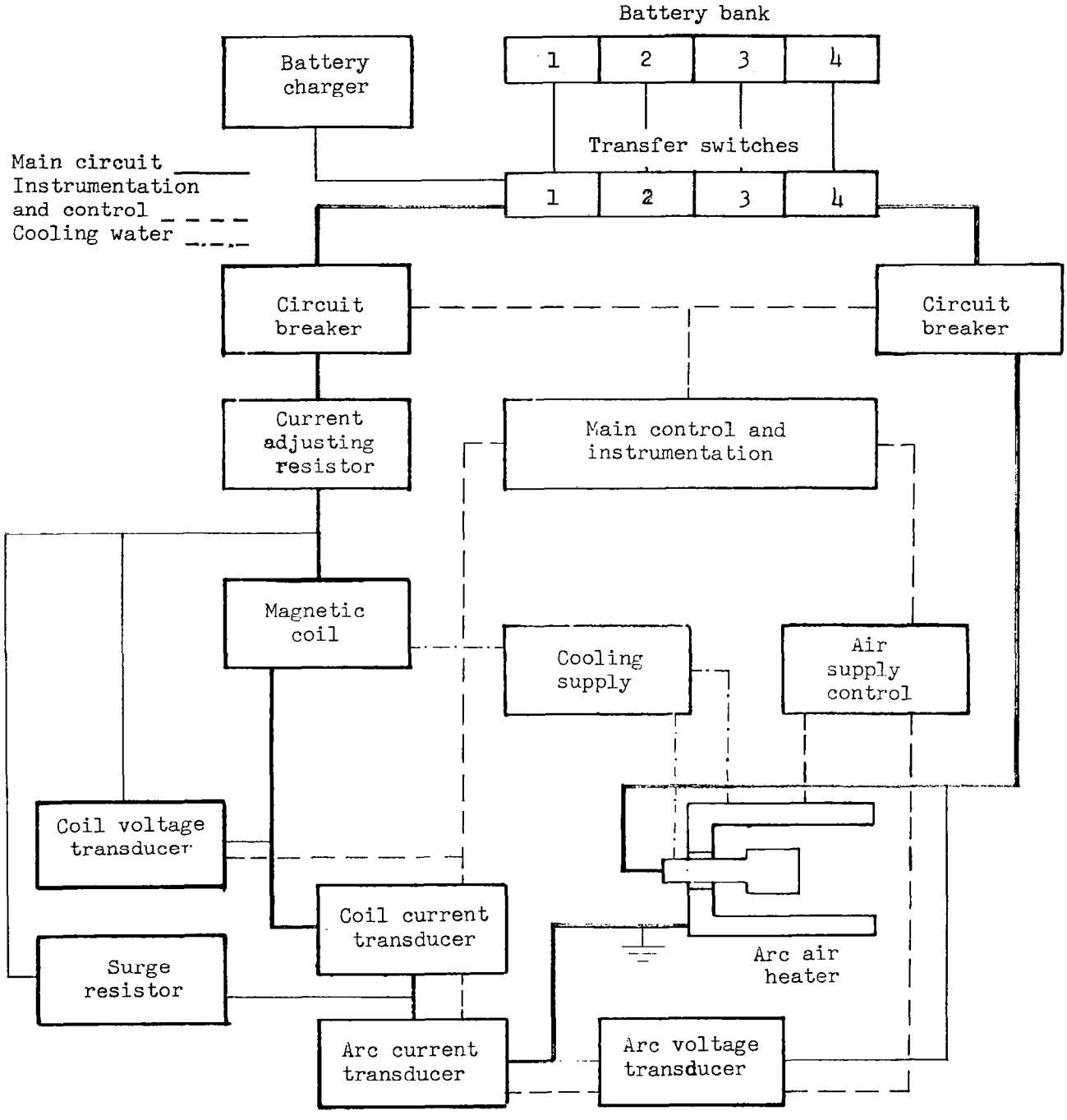

Figure 3.- Schematic diagram of arc air heater electrical, cooling water, and control systems.

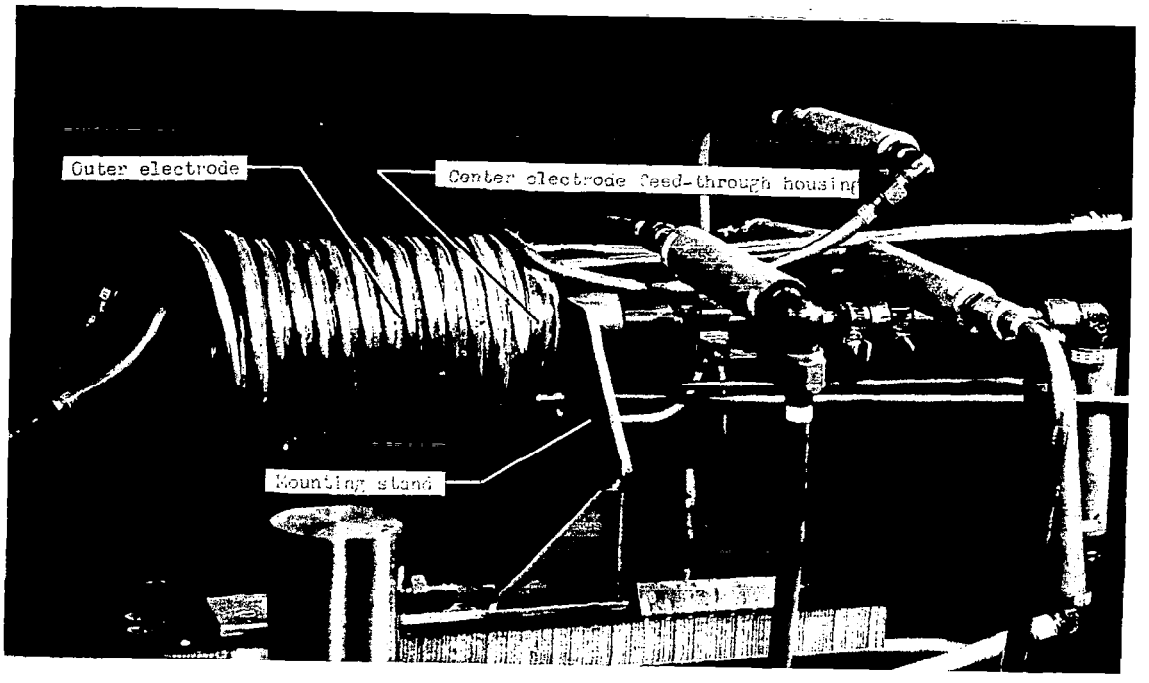

L-60-97.1

Figure 4.- Combined outer electrode and pressure vessel with cooling tubes shown mounted.

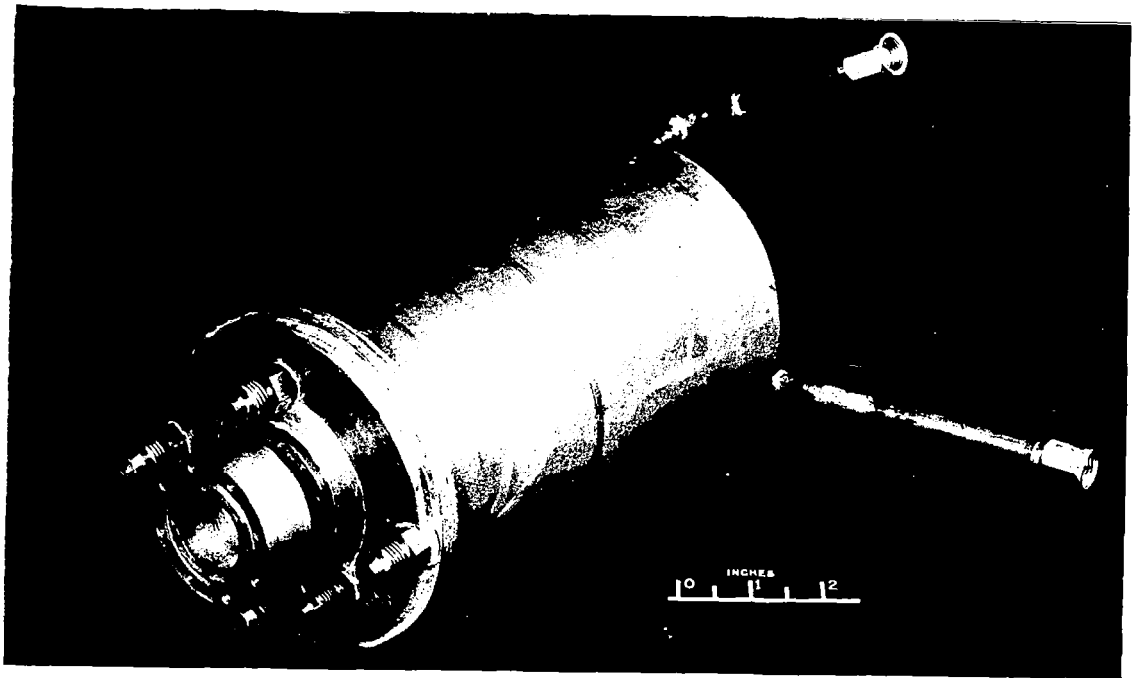

L-61-5182

Figure 5.- Arc air heater combined outer electrode and pressure vessel with internal cooling passages.

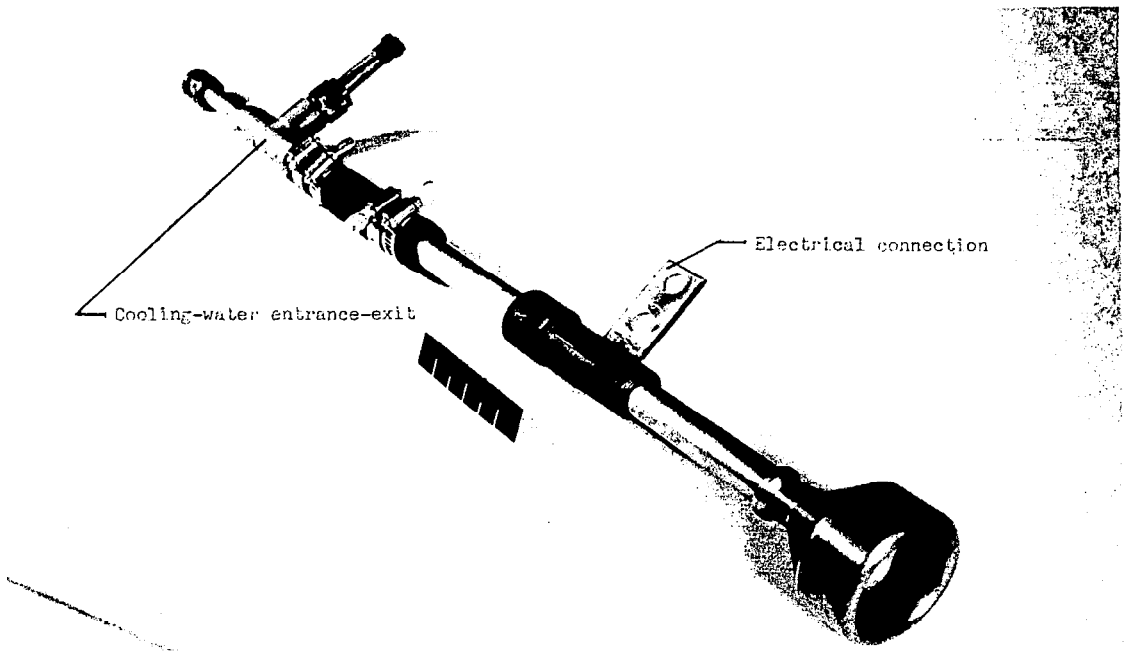

L-60-4407.1

(a) Electrode showing electrical connections and water entrance-exit connection.

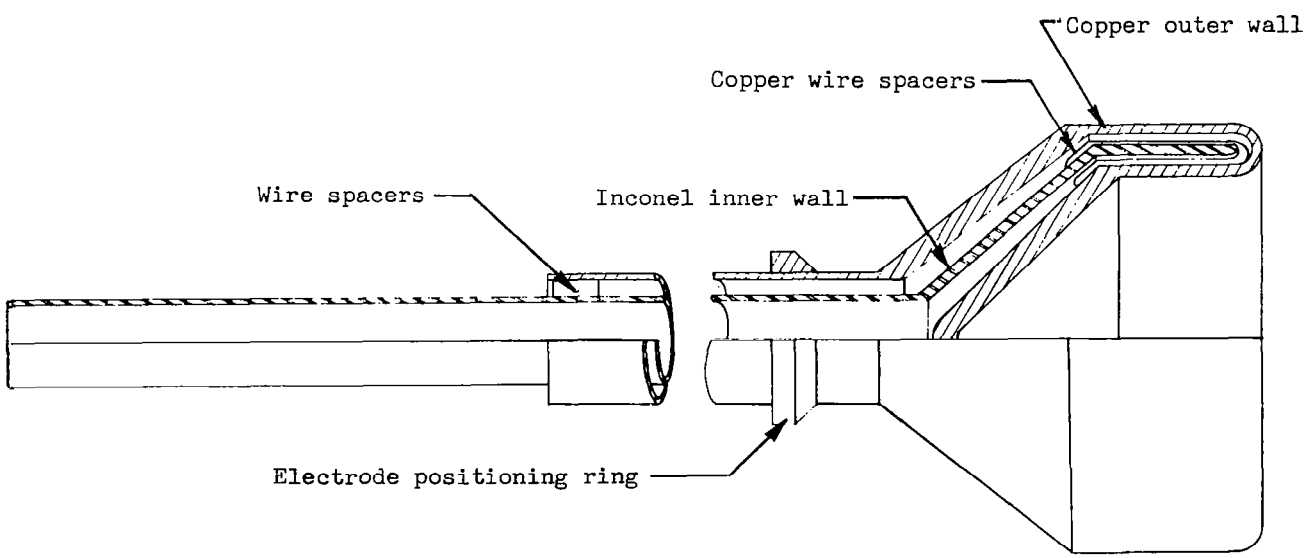

(b) Section view of center electrode.

Figure 6.- Water-cooled cup-shaped center electrode.

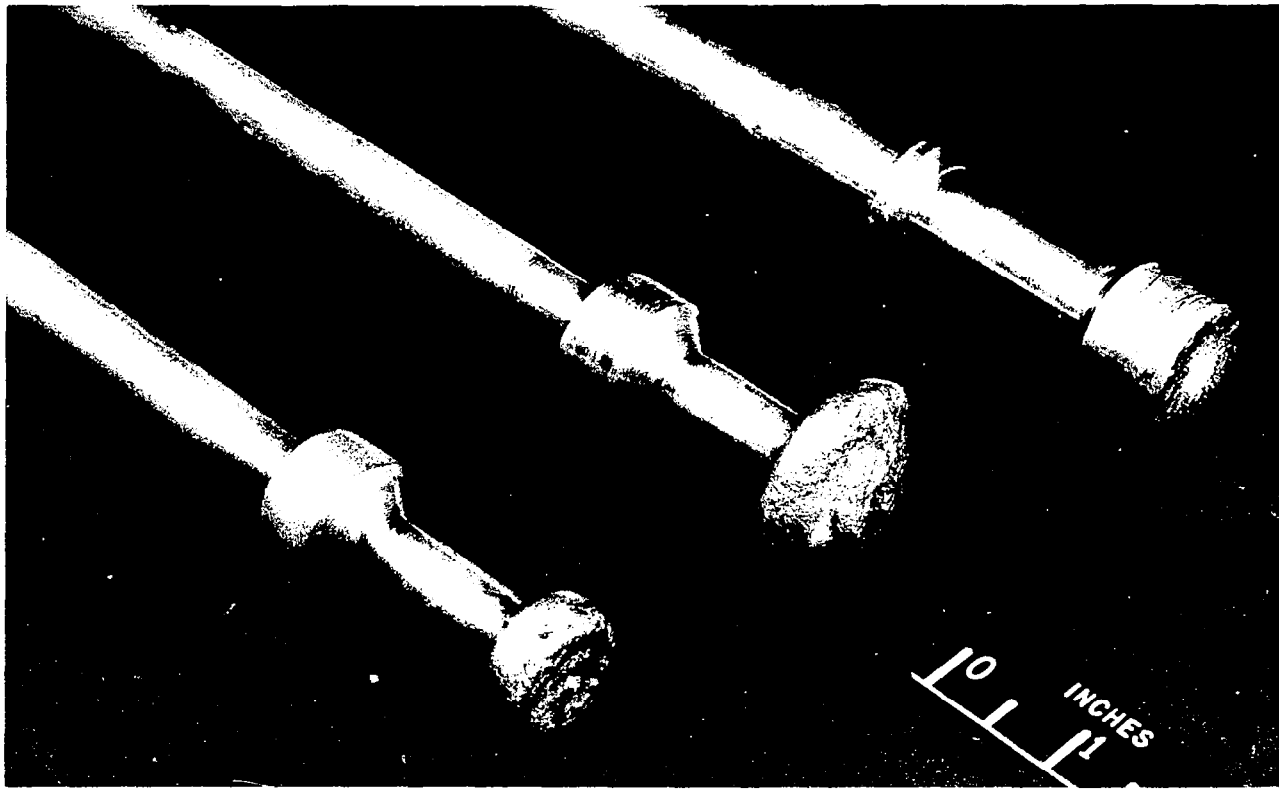

L-61-5179

Figure 7.- Water-cooled copper disk electrodes showing failure due to arc attachment at the center.

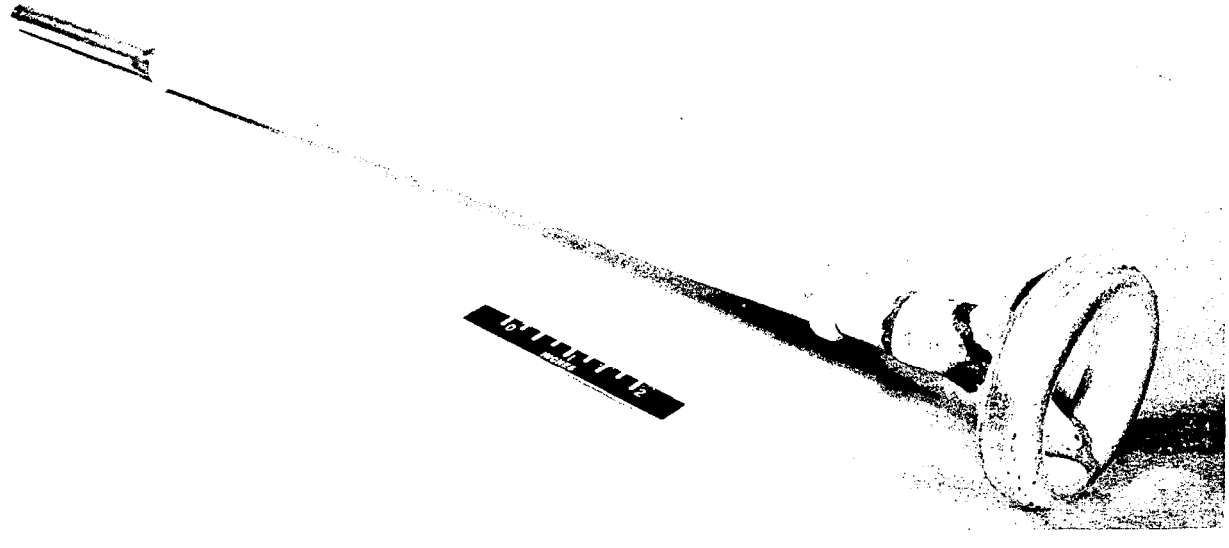

Figure 8.- Water-cooled copper toroid center electrode. L-61-3757

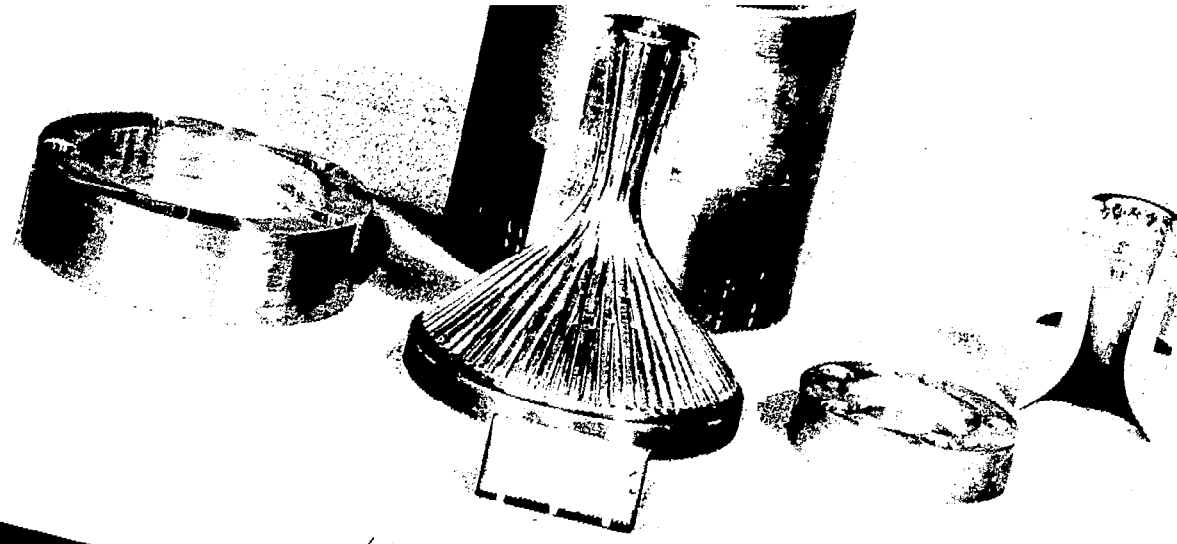

(a) Nozzle before assembly.

L-60-6754

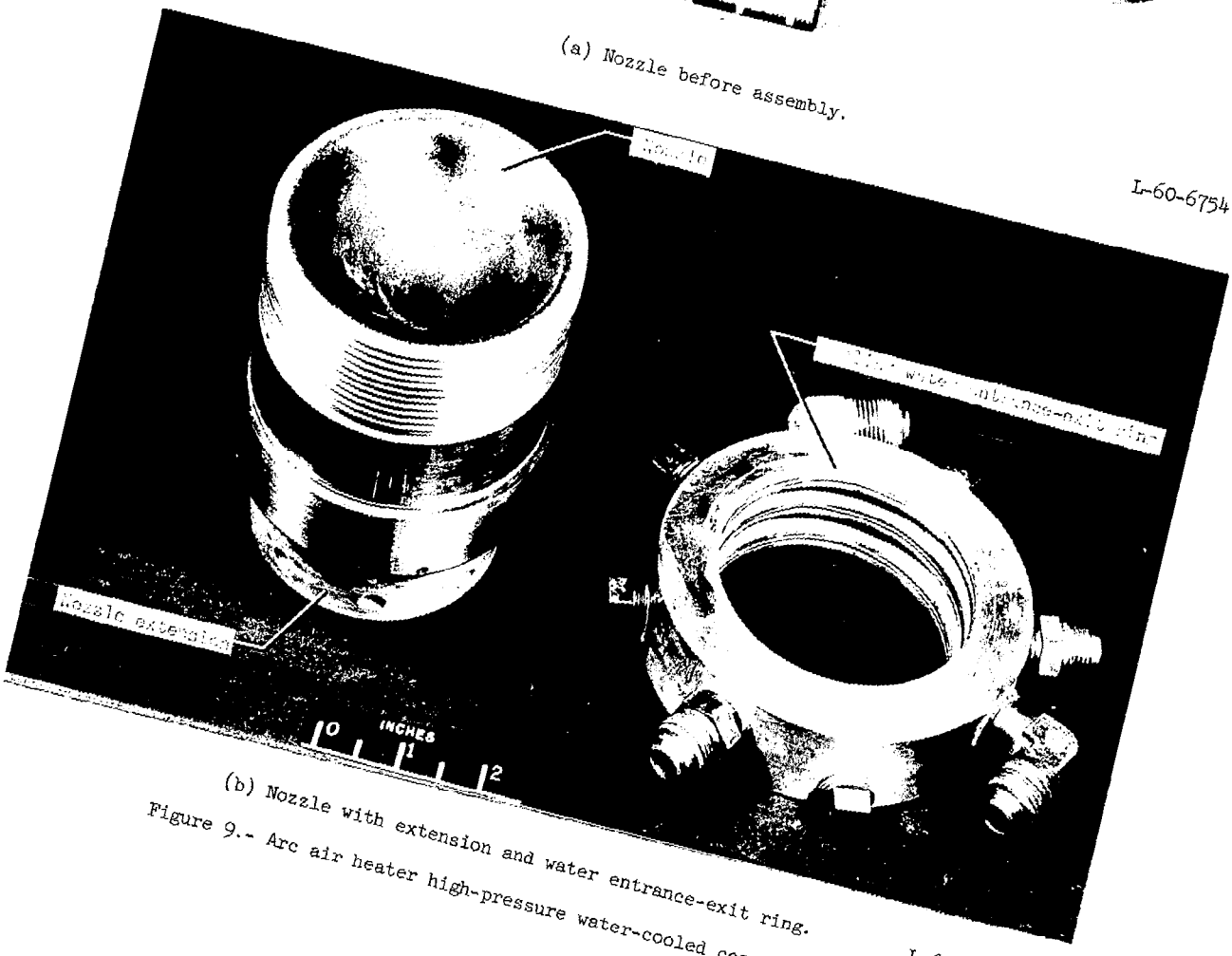

(b) Nozzle with extension and water entrance-exit ring.

L-61-5183.1

Figure 9.- Arc air heater high-pressure water-cooled copper nozzle.

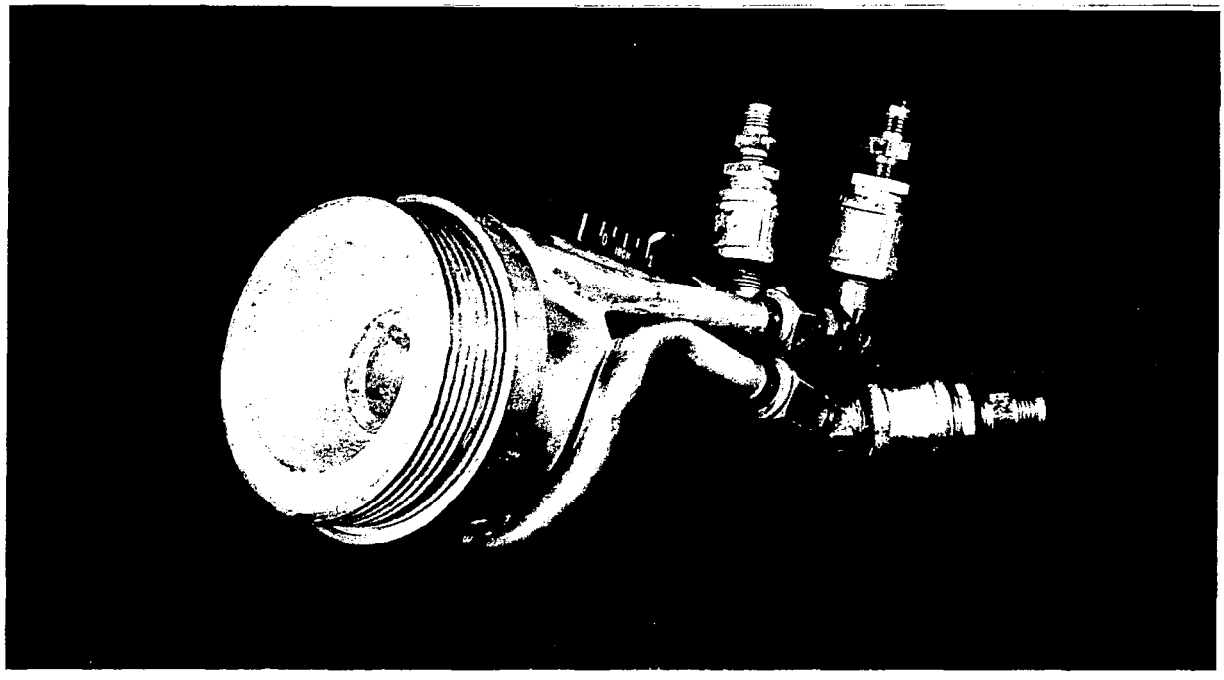

Figure 10.- Arc air heater low-pressure water-cooled copper nozzle. L-60-8361

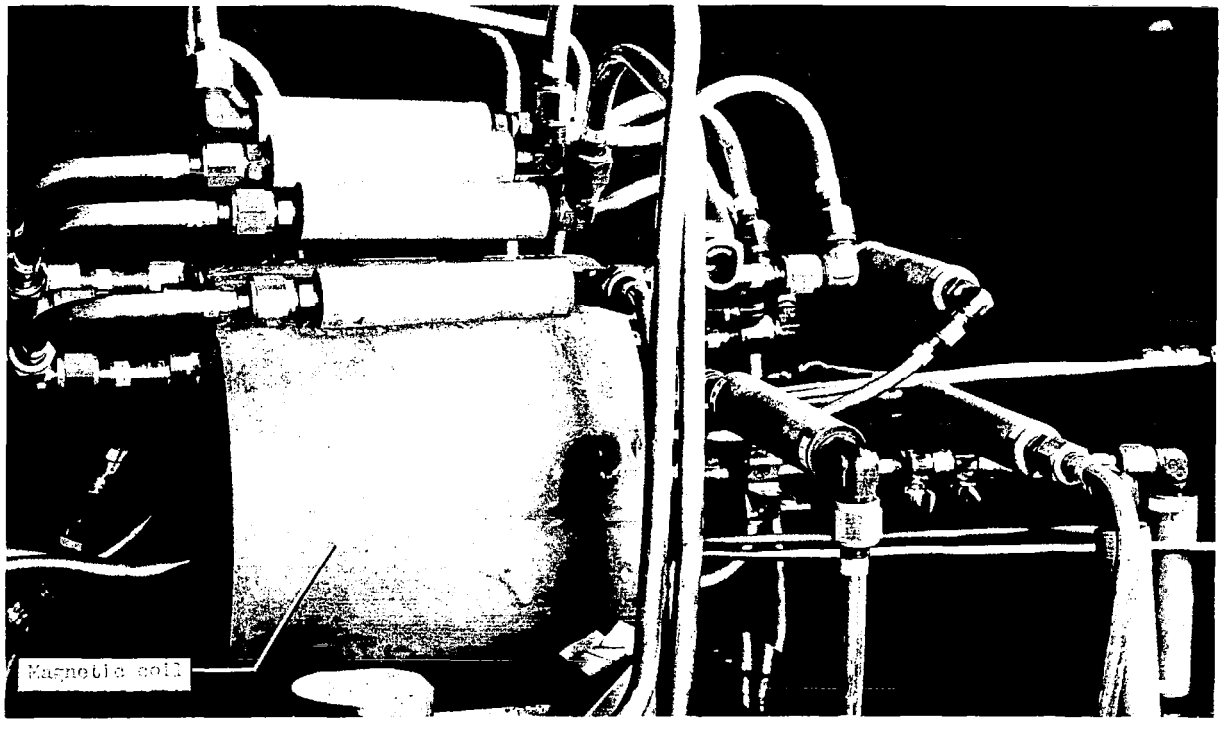

Figure 11.- Arc air heater with layer-type magnetic coil. L-60-95.1

Figure 12.- Power supply for arc air heater.

L-61-3750

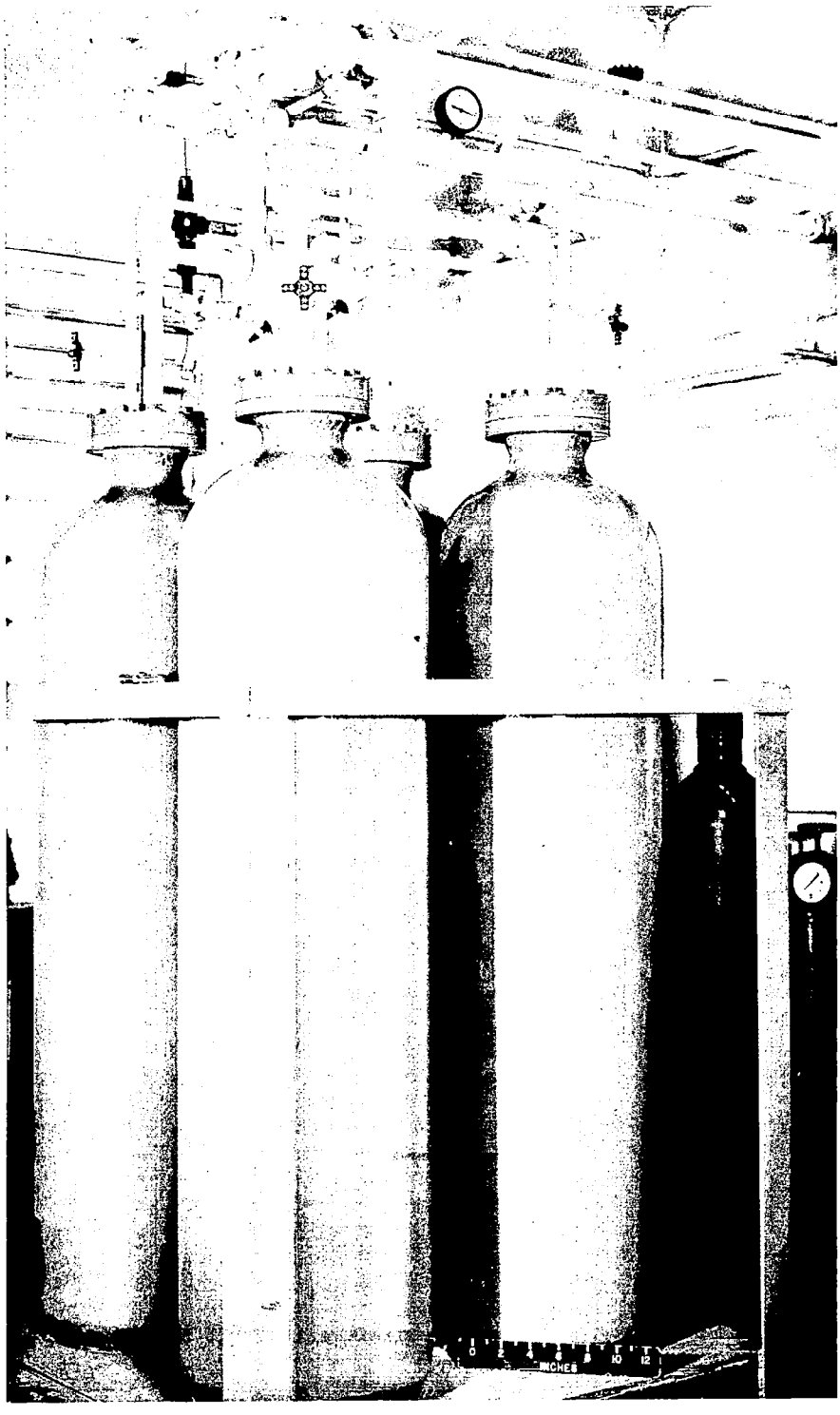

L-61-3756

Figure 13.- Cooling water supply and return bottles for arc air heater and magnetic coil.

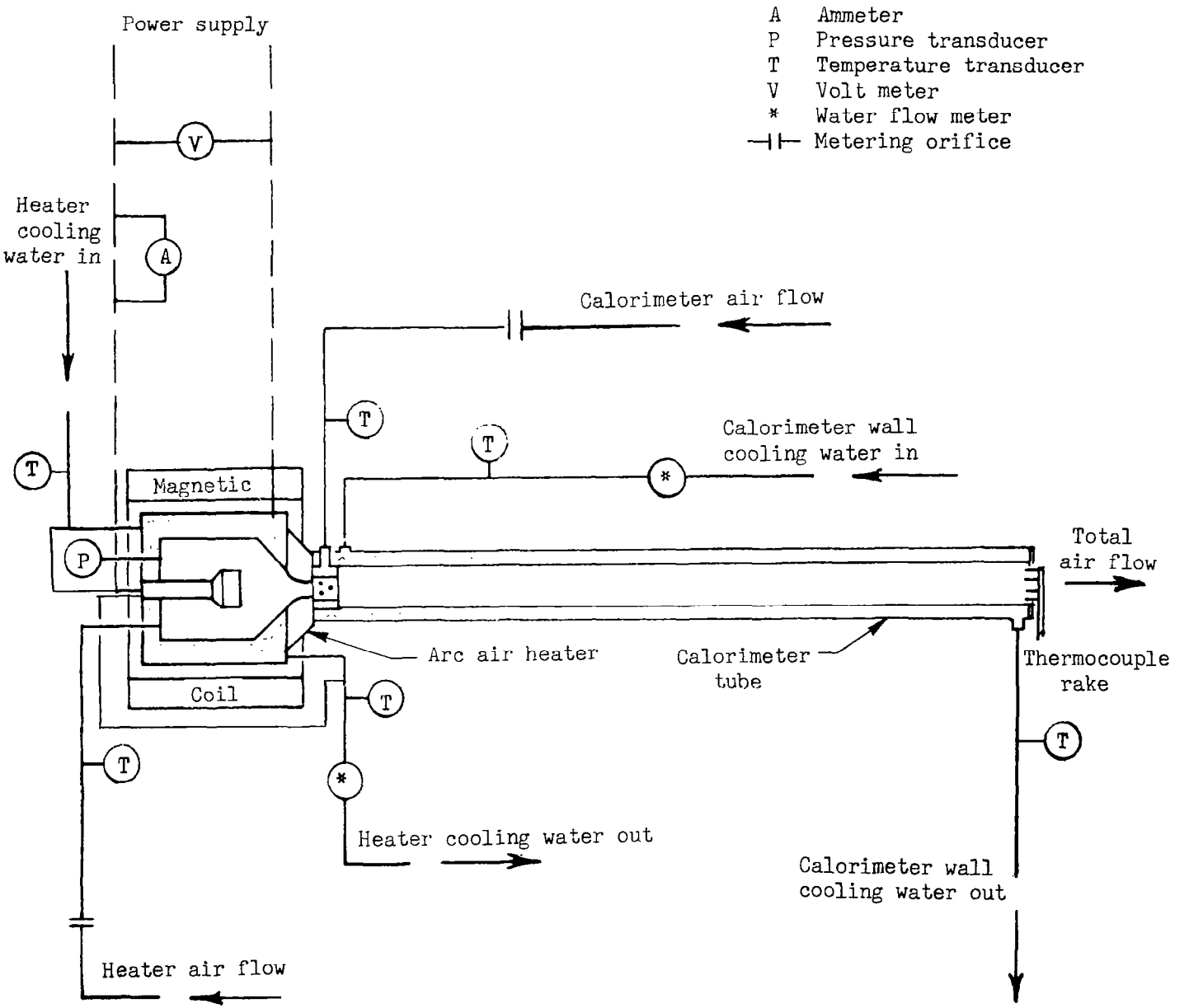

Figure 14.- Diagram of arc air heater with calorimeter.

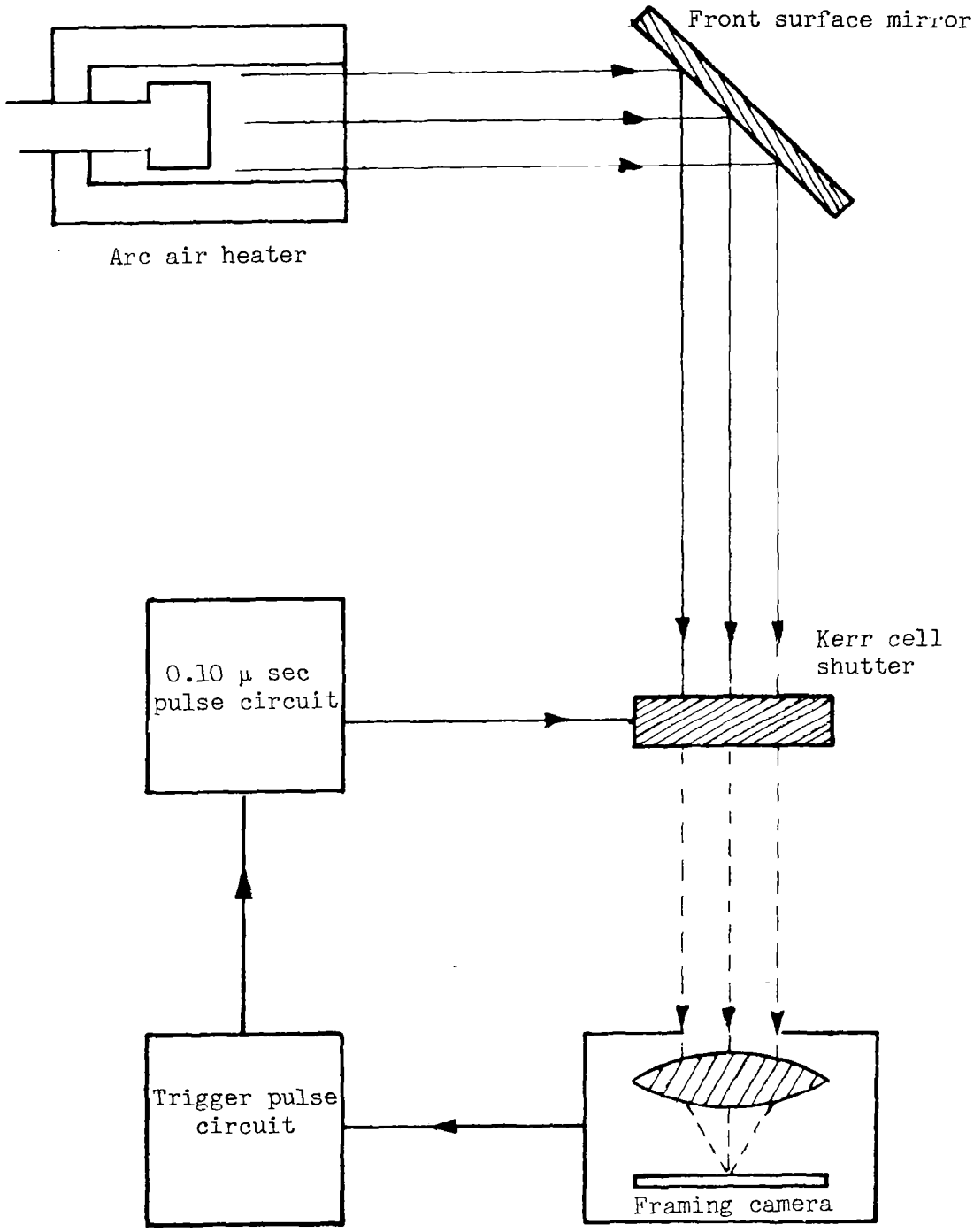

Figure 15.- Kerr cell shutter and framing camera arrangement.

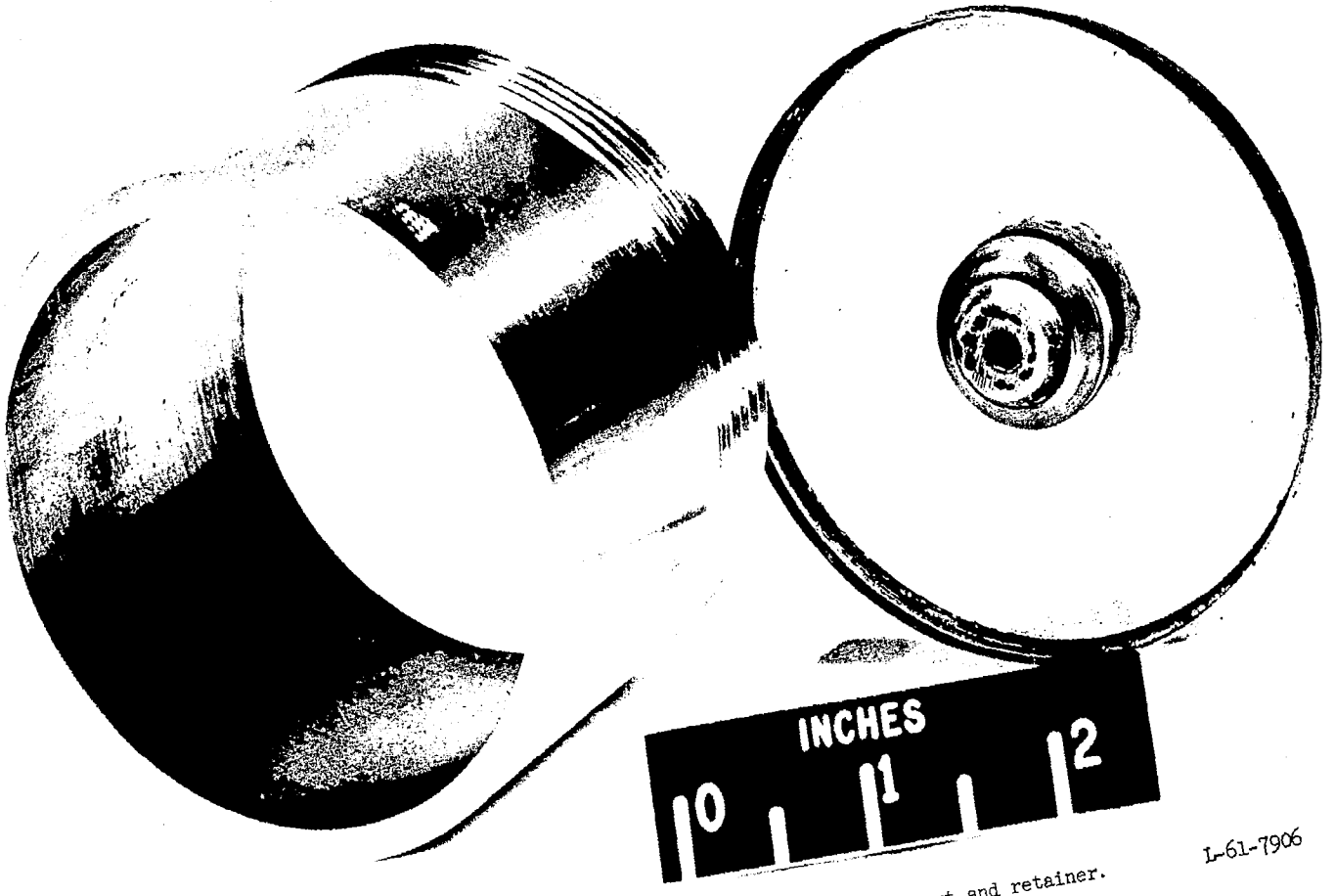

L-61-7906

Figure 16.- Transparent window with nozzle insert and retainer.

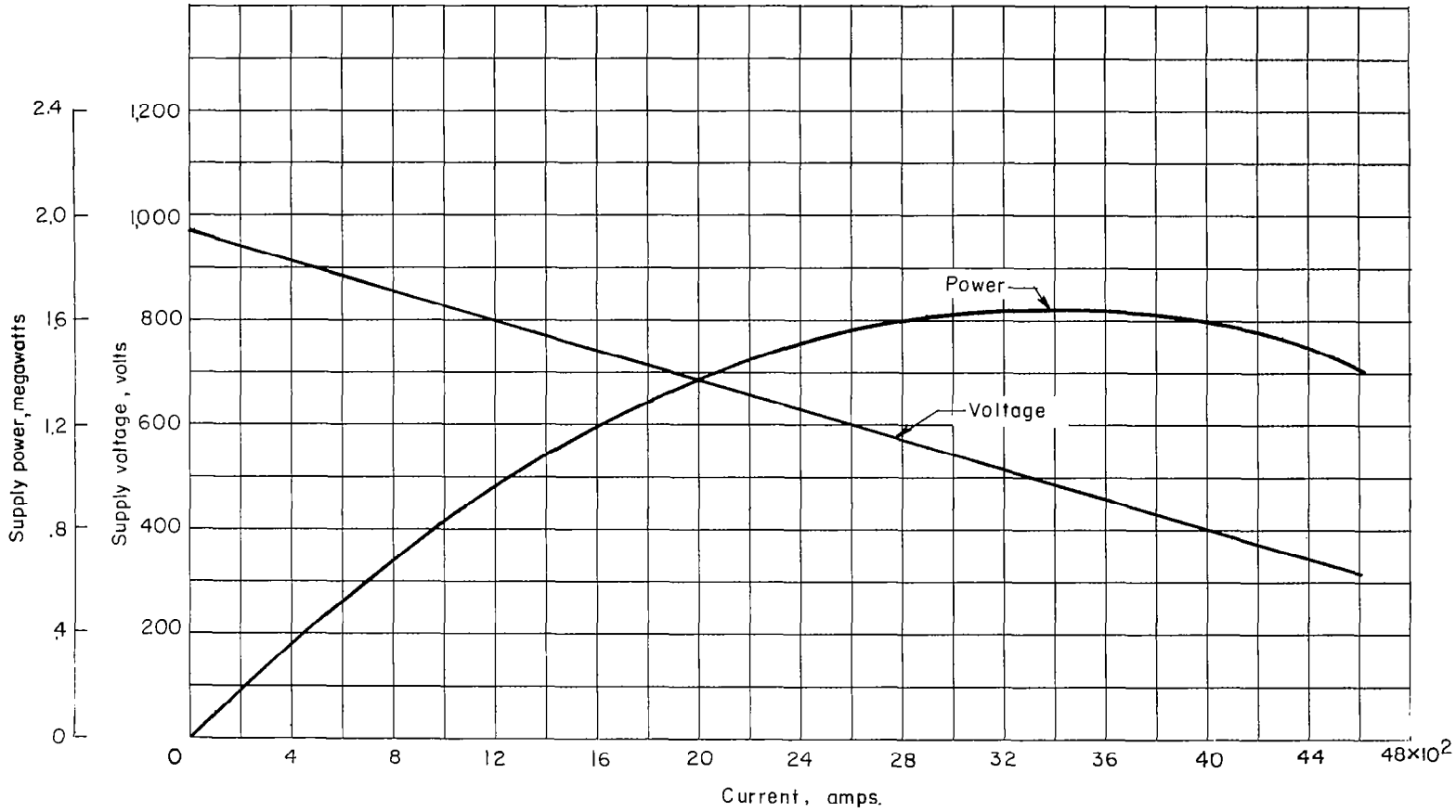

Figure 17.- Arc air heater power-supply characteristics.

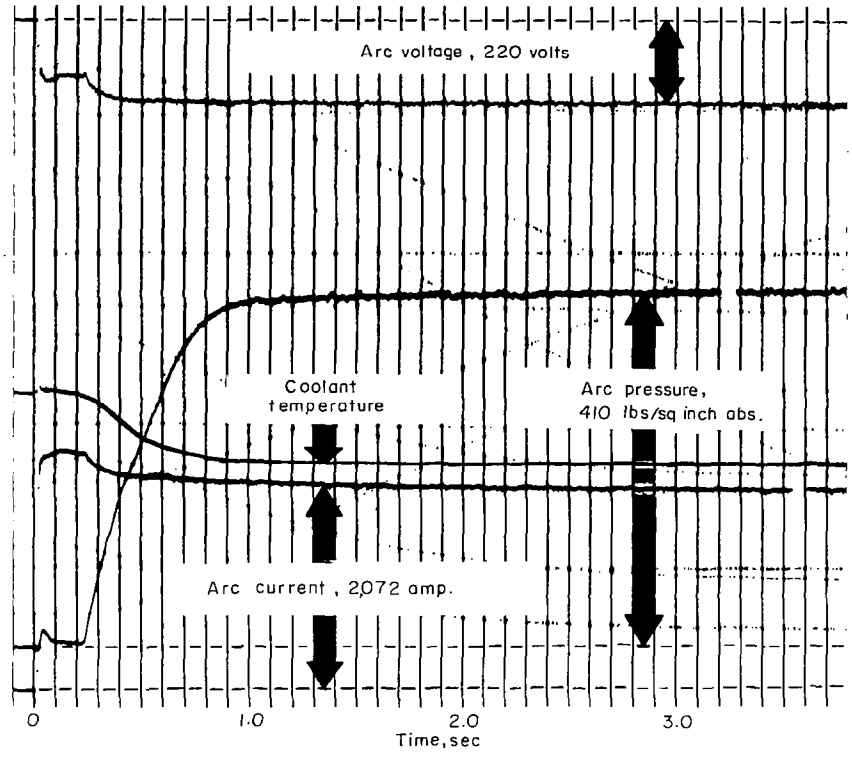

Figure 18.- Arc air heater starting characteristics.

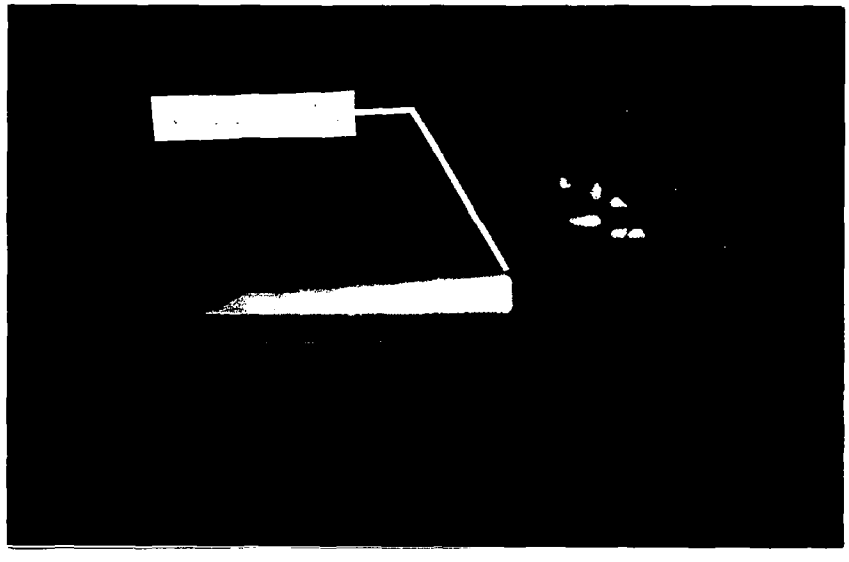

L-63-4739

Figure 19.- View of arc air heater operating. Atmospheric exit 944 kw to electrodes; 600 lb/sq in. abs arc chamber pressure; 16,000 gauss magnetic flux; 1.0-inch nozzle exit diameter; 0.2-inch nozzle throat diameter; 0.102 lb/sec air mass flow.

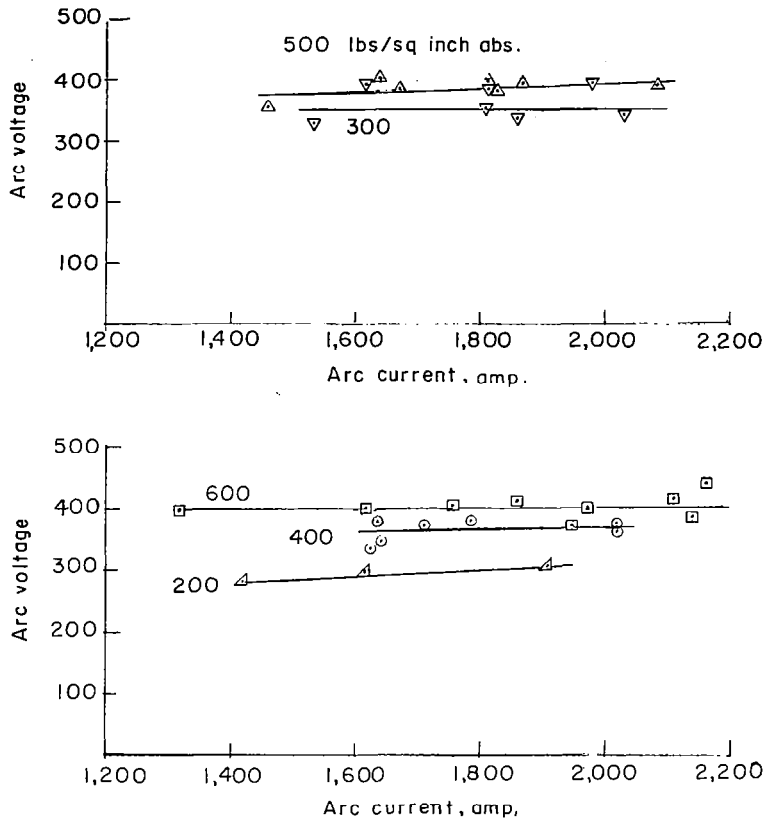

Figure 20.- Arc voltage and current relationship for various arc chamber pressures. Arc gap, 7/16 inch; $\frac{B}{I} = 7.5 \frac{\text{gauss}}{\text{amp}}$.

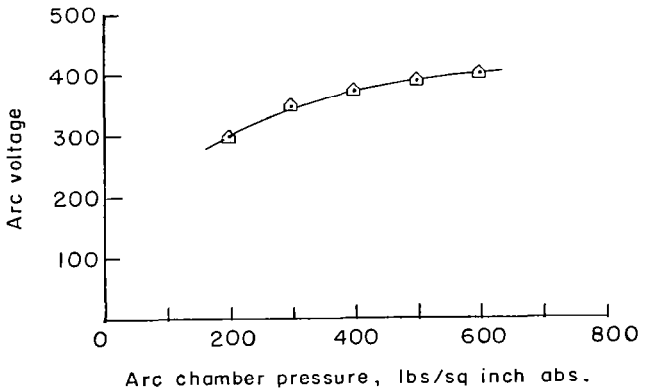

Figure 21.- Arc voltage and pressure relationship. Arc gap, 7/16 inch; arc current, 1,750 amp.

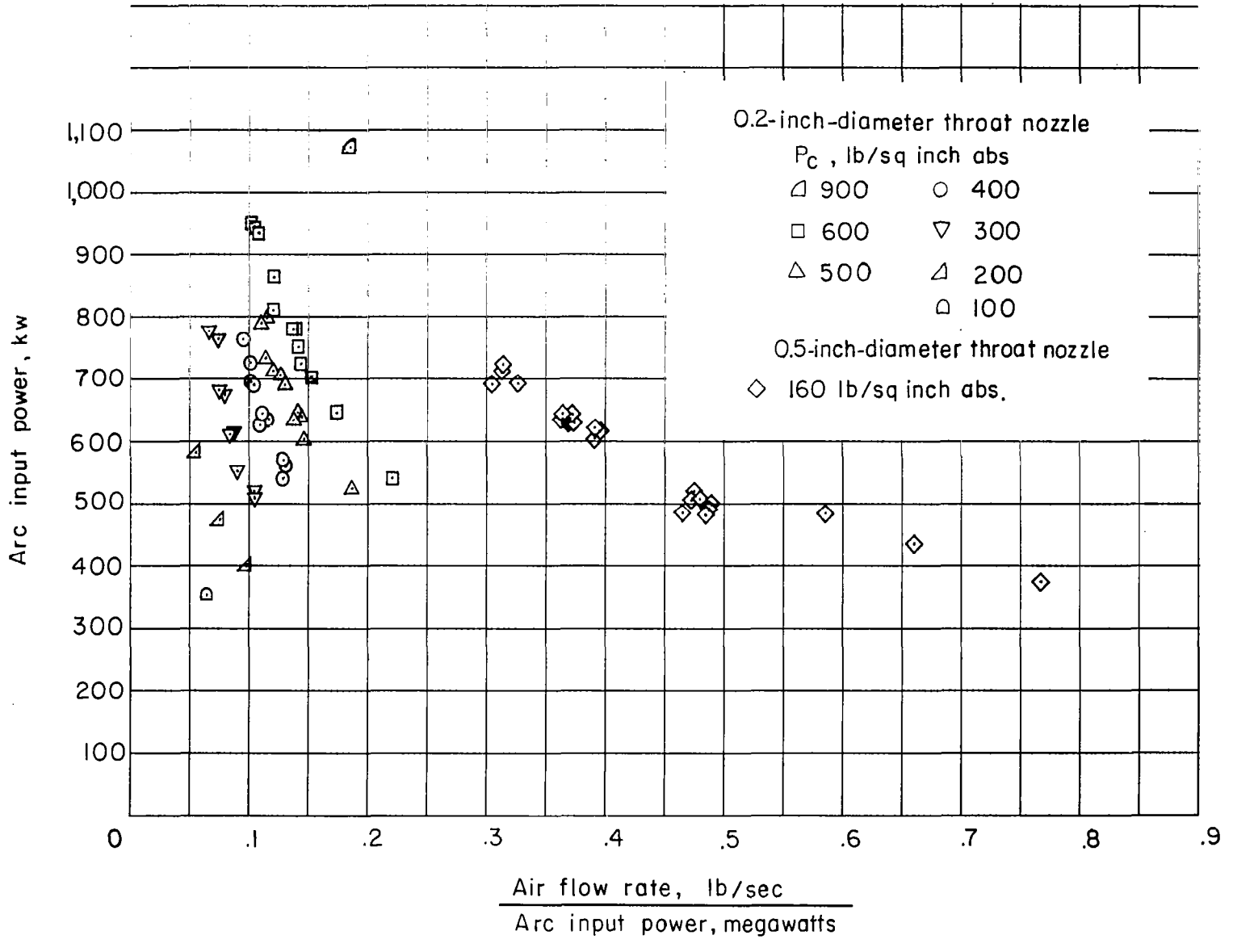

Figure 22.- Actual values of arc air heater input conditions.

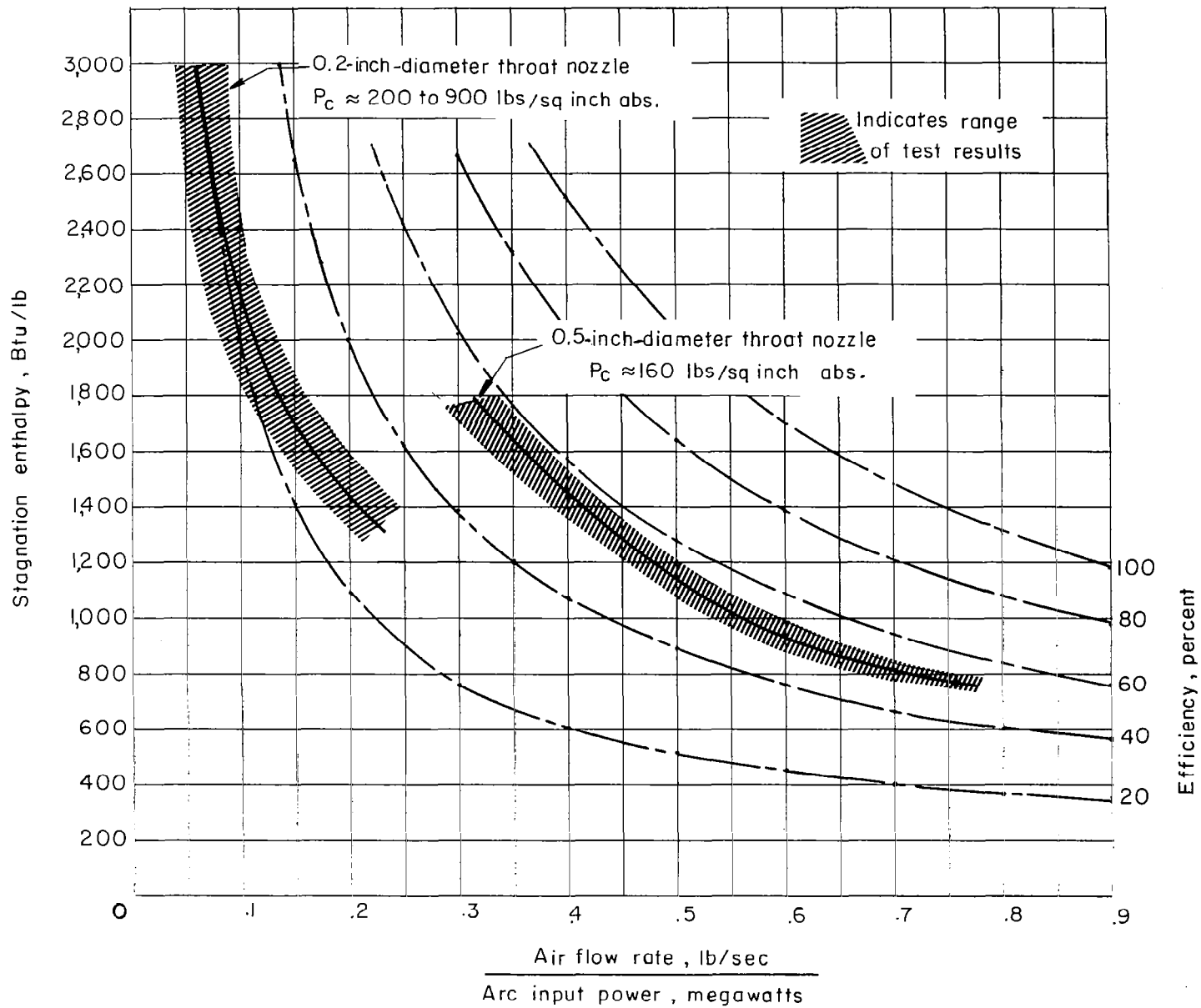

Figure 23.- Arc air heater stagnation air enthalpy curve. Efficiency curves indicate heater efficiency required to produce a given enthalpy for air entering at 60° F.

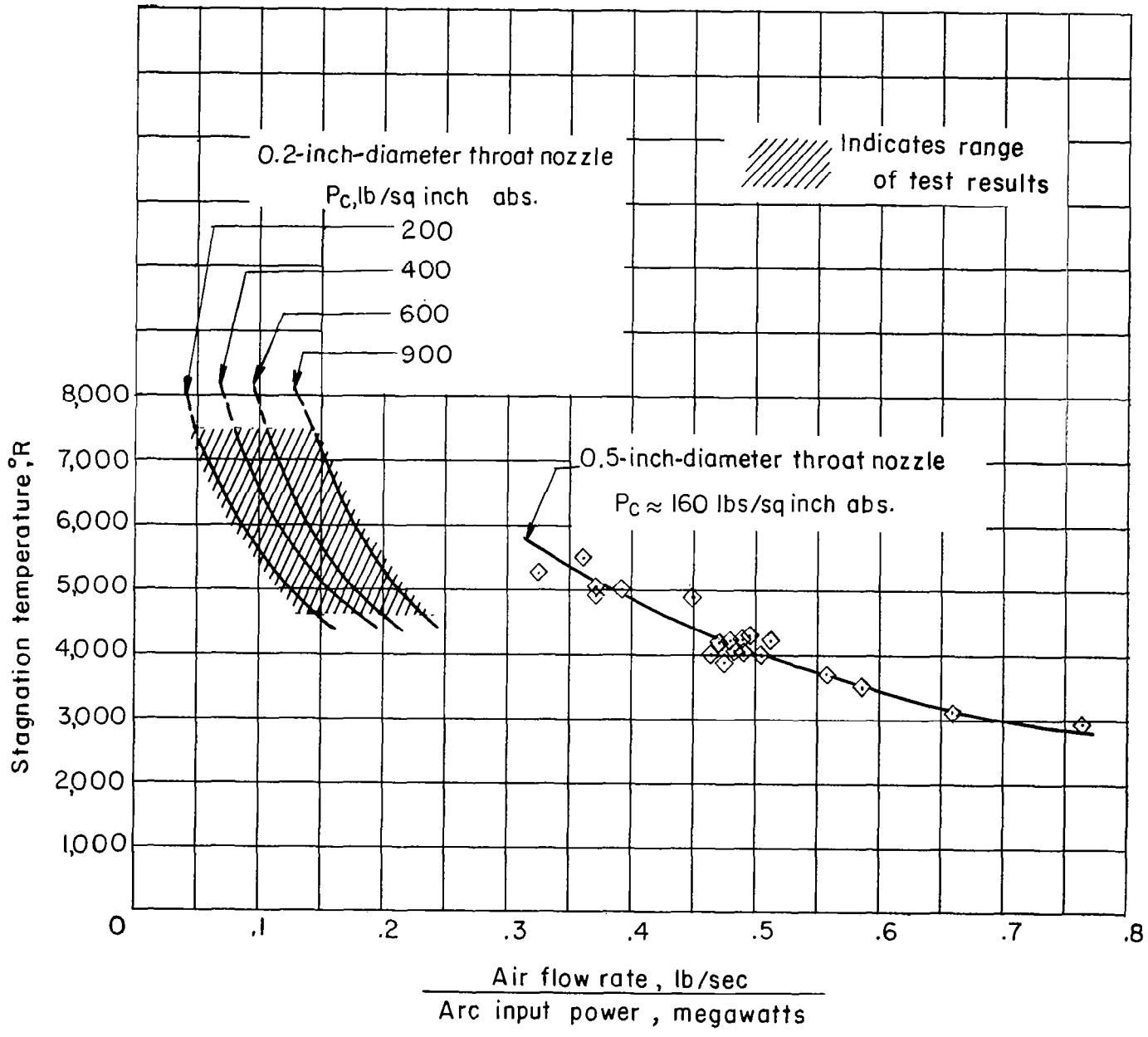

Figure 24.- Arc air heater stagnation air temperature curve.

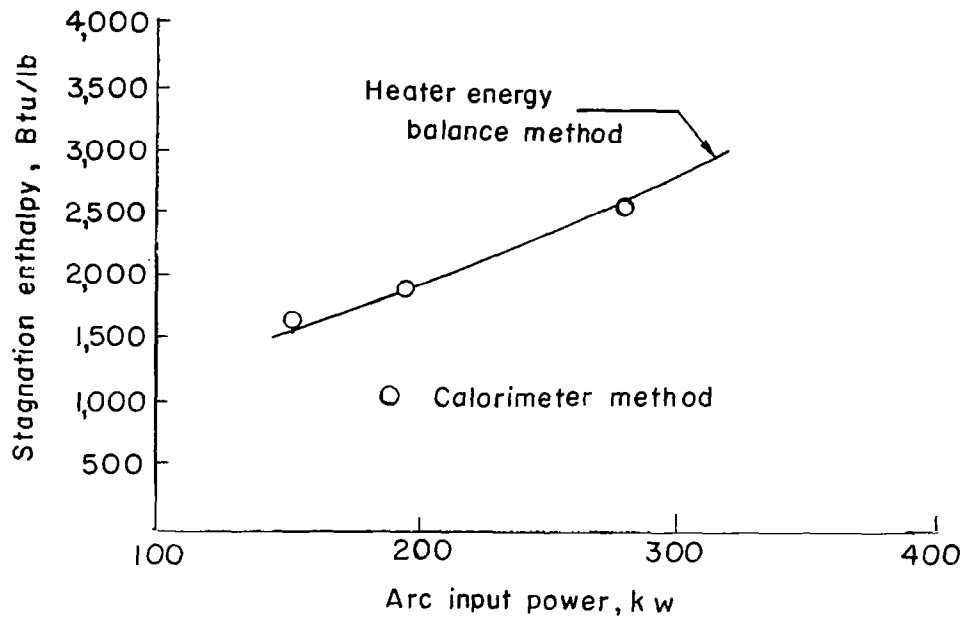

Figure 25.- Comparison of arc air heater stagnation and air enthalpy values.

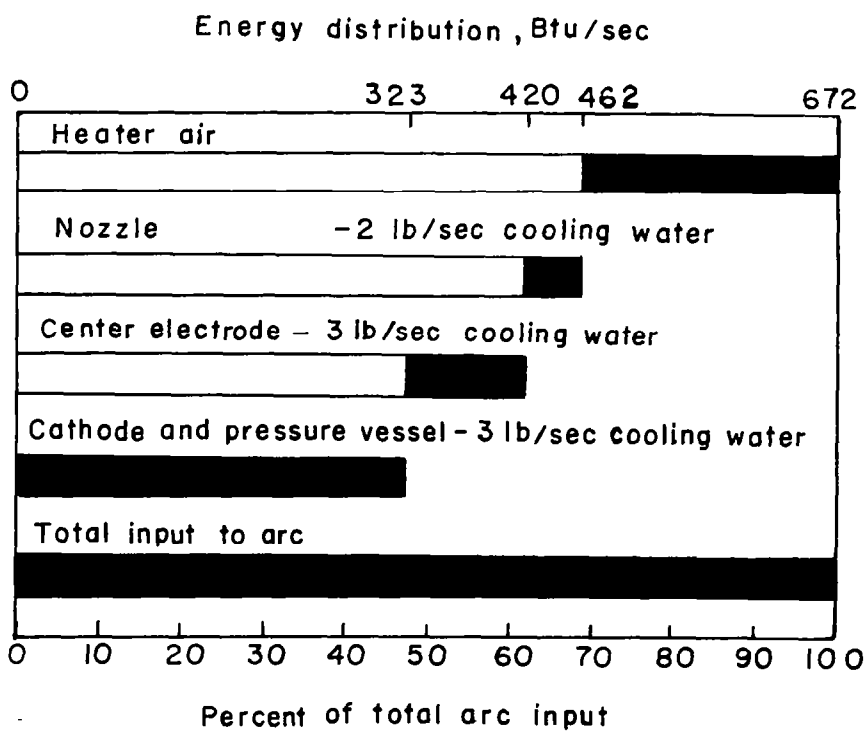

Figure 26.- Arc air heater energy and cooling distribution. P_c = 598 lb/sq in. abs.

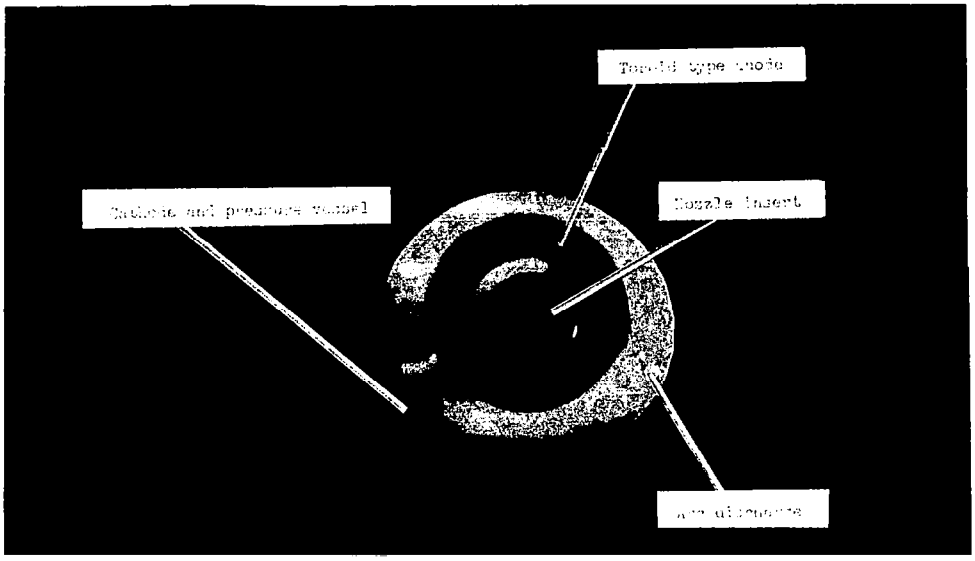

L-63-4740

Figure 27.- Photographic view of arc discharge. 43 μsecond exposure; arc current, 2,600 amp; arc pressure, approximately 55 lb/sq in. abs (air); magnetic flux, >19,500 gauss.

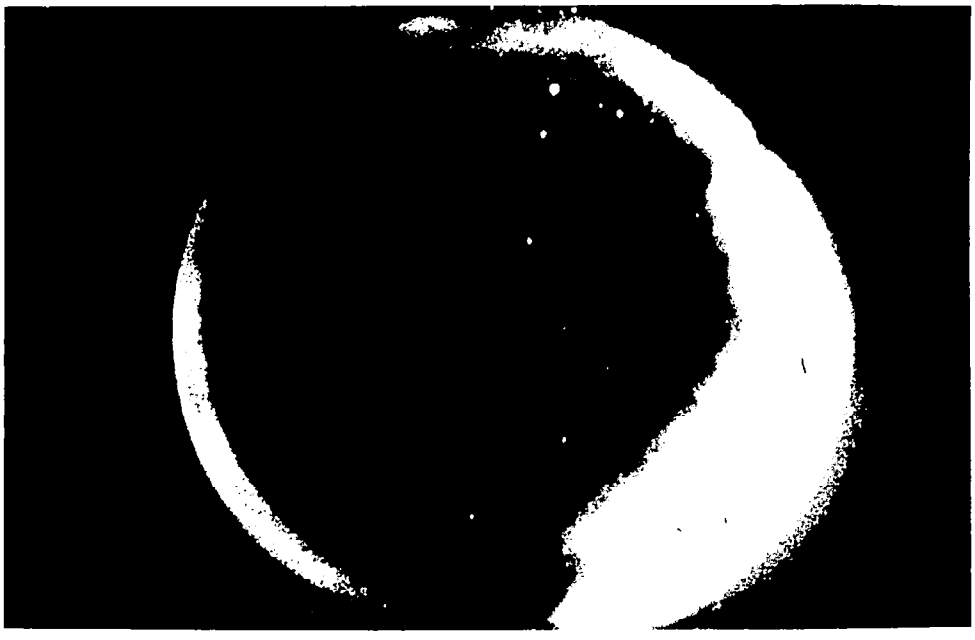

L-63-4741

Figure 28.- Photographic view of arc discharge. 43 μsecond exposure; arc current, 1,200 amp; arc pressure, atmospheric; magnetic flux, 9,000 gauss.

L-63-4742

L-63-4743

Figure 29.- Variations in arc discharge during a run. 0.1 μsecond exposure; arc current, 2,040 amp; arc pressure, atmospheric; magnetic flux, 15,300 gauss.

L-63-4744

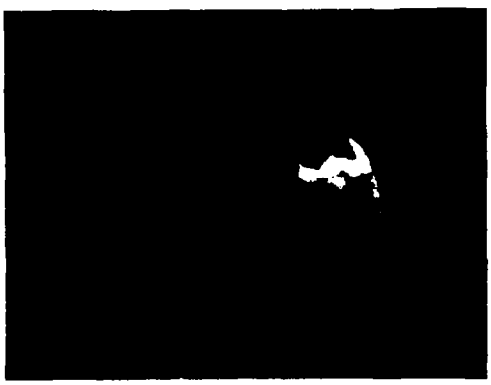

Figure 29.- Concluded.

L-63-4745

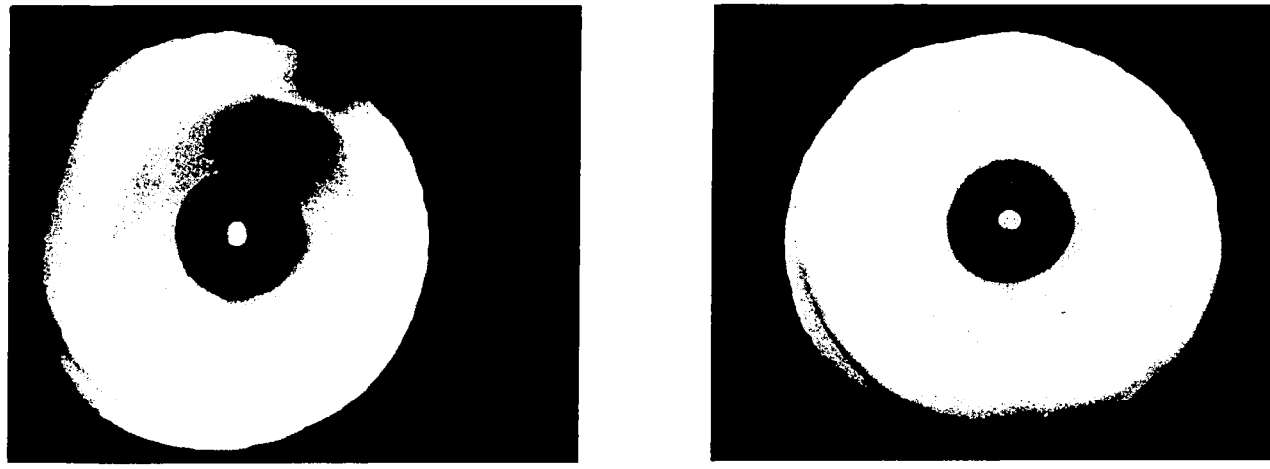

L-63-4746

Figure 30.- Photographic view of arc discharge. 43 μsecond exposure; arc current, 1,800 amp; arc pressure, 600 lb/sq in. abs (air); magnetic flux, 13,500 gauss.

L-63-4747

Figure 31.- Variations in arc discharge during a run. 0.1 μsecond exposure; arc current, 1,800 amp; arc pressure, 600 lb/sq in. abs (air); magnetic flux, 13,500 gauss.

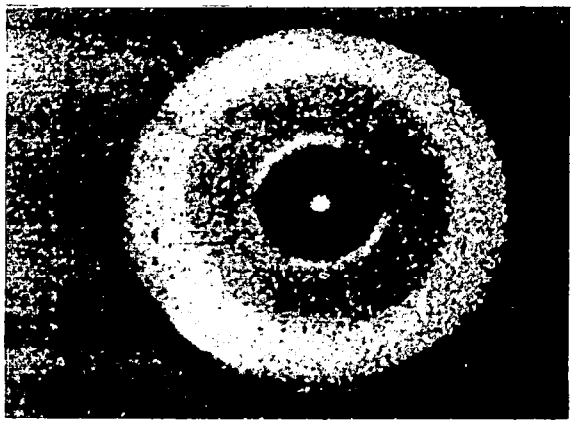

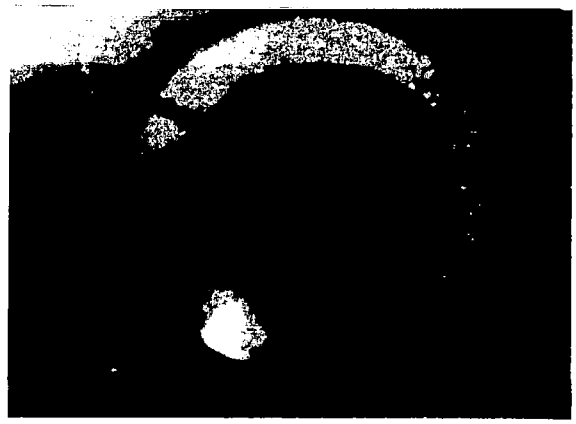

L-63-4748

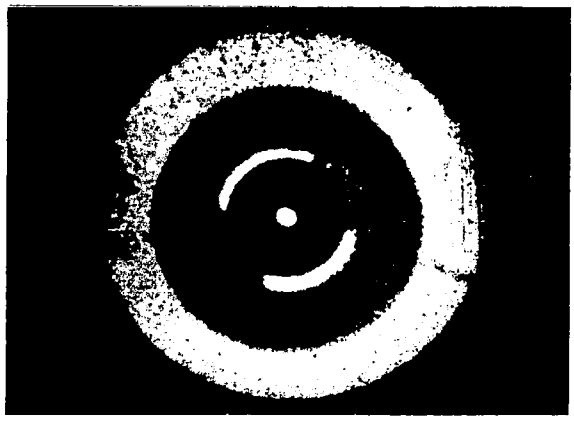

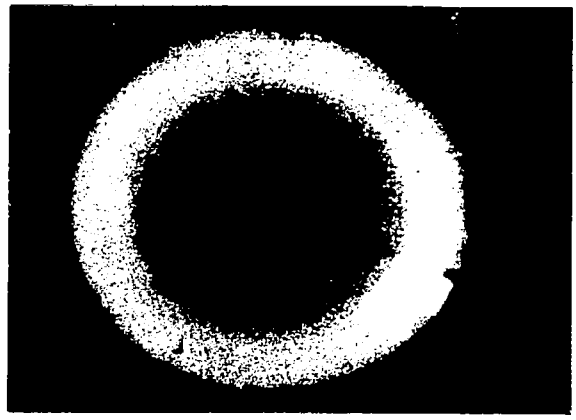

Figure 31.- Continued.

L-63-4749

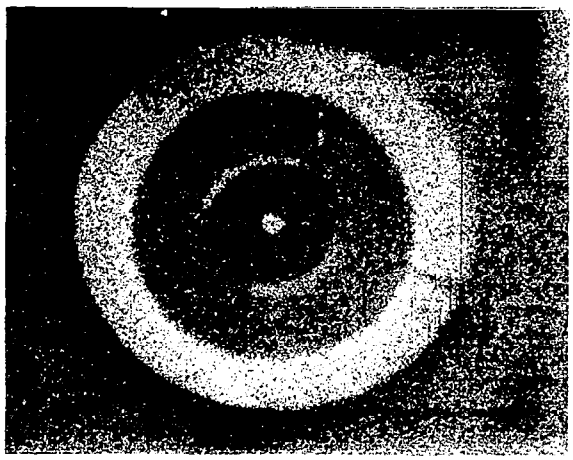

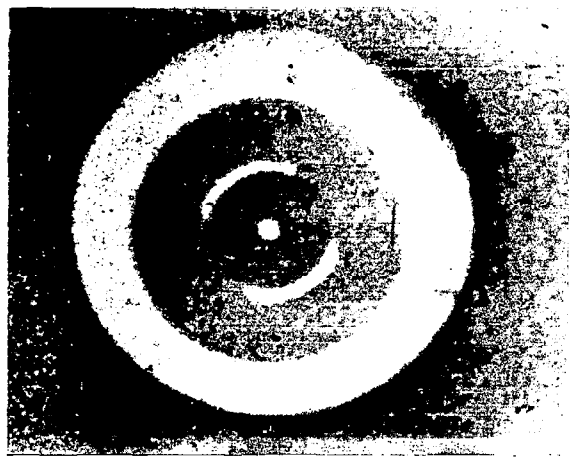

L-63-4750

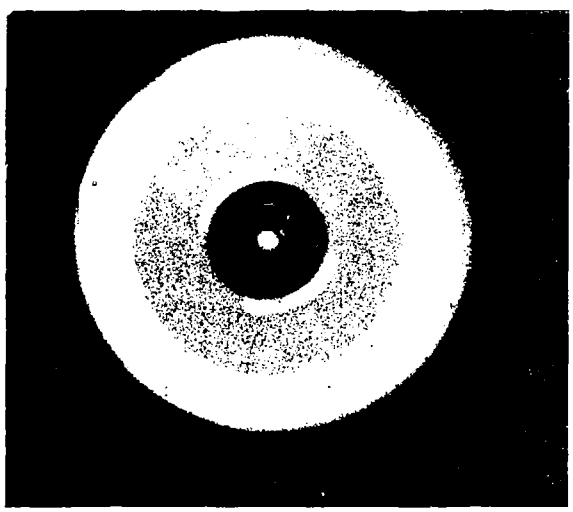

L-63-4751

Figure 31.- Concluded.

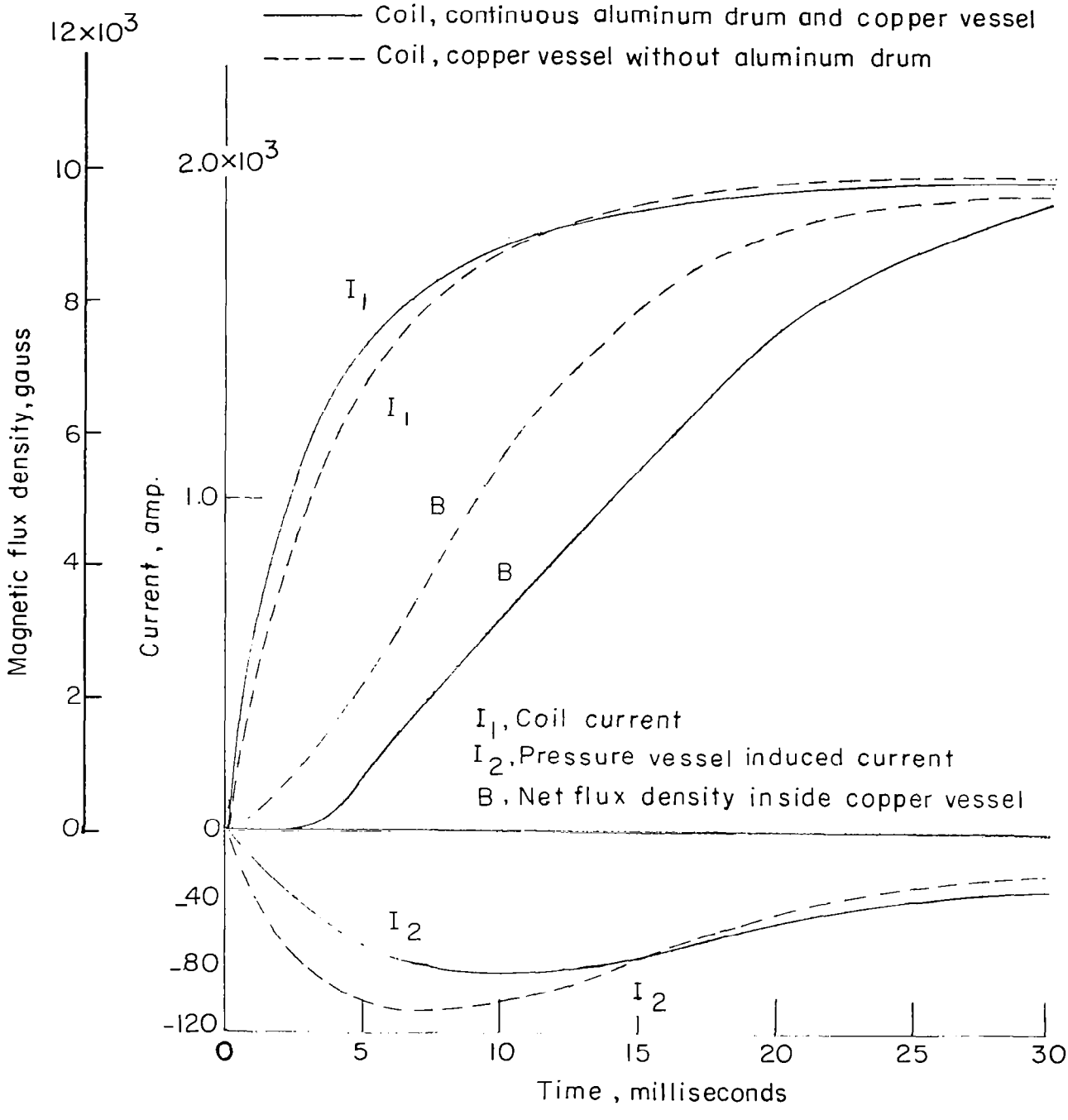

Figure 32.- Calculated transient response of simplified arrangement upon initial application of voltage.